Part I

Temporary Overvoltages in IBRs Connected Power Systems

Saeed Lotfifard
Hassan Yazdani, Graduate Student

Washington State University

For information about this project, contact

Saeed Lotfifard
Washington State University
School of Electrical Engineering and Computer Science
Pullman, Washington 99164-2752
Phone: 509-335-0903
Email: s.lotfifard@wsu.edu

Power Systems Engineering Research Center

The Power Systems Engineering Research Center (PSERC) is a multi-university Center conducting research on challenges facing the electric power industry and educating the next generation of power engineers. More information about PSERC can be found at the Center's website: http://www.pserc.org.

For additional information, contact:

Power Systems Engineering Research Center
Arizona State University
527 Engineering Research Center
Tempe, Arizona 85287-5706
Phone: 480-965-1643
Fax: 480-727-2052

Notice Concerning Copyright Material

Table of Contents

List of Figures

List of Tables

NOMENCLATURE

Acronym

CSCR	Composite short circuit ratio
ESCR	Equivalent short circuit ratio
GFL	Grid following
GNC	Generalized Nyquist criterion
GSIM	Grid strength impedance metric
HVdc	High-voltage direct current
IBR	Inverter-based resource
IILSCR	Short circuit ratio with interaction levels
LVRT	Low voltage ride through
MESCR	Multi-infeed effective short circuit ratio
MIIF	Multi-infeed interaction factor
MISCR	Multi-infeed short circuit ratio
POI	Point of interconnection
SCC	Short circuit capacity
SCR	Short circuit ratio
SDSCR	Site-dependent short circuit ratio
TOV	Temporary overvoltage
WSCR	Weighted short circuit ratio

Parameters

$Z_g;\ Z_b$	Grid's equivalent impedance and base impedance, respectively
$I_d^{ref};\ I_q^{ref}$	Reference values of the IBR controller on each axis
$I_G; I_R$	Set of branch currents with conventional generators and IBRs, respectively
$I_{max};\ V_{max}$	Maximum current and voltage of the IBR, respectively
I_N	Nominal current of the IBR
$k_p^{PLL};\ k_i^{PLL}$	Proportional and integral coefficients of the PI PLL controller, respectively

$k_p;\ k_i$	Proportional and integral coefficients of the PI current controller, respectively
MV_{IBR}	Sum of nominal MW of existing IBRs
$P_{dc}; Q_{dc}$	Nominal active/reactive power of the HVdc plant
P_R	Rated MW of the IBR to be connected
Q_c	Shunt compensation of reactive power
$R_f; L_f; C_f$	Resistance, inductance, and capacitance of the IBR filter, respectively
$R_g;\ L_g$	Thevenin equivalent of the grid resistance and inductance
S_{SC}	SCC prior to IBR integration
U_i	Rated voltage at bus i
$V_G;\ V_R$	Set of bus voltages with conventional generators and IBRs, respectively
$Z_{BUS}; z_{i,j}$	Grid's impedance matrix and its ij-th element, respectively
$Z_{GG}; Z_{RR}$	Subsets of the grid's impedance matrix with conventional generators and IBRs, respectively
$Z_{GR};\ Z_{RG}$	Subsets of the grid's impedance matrix with both conventional generators and IBRs, respectively
Z_{IBR}	Equivalent impedance behavior of the IBR

Operators

$\mathbf{T}_{dq}$	dq transformation matrix
$J;\ J_R$	Jacobian and reduced Jacobian matrices, respectively
$\Phi;\ \Gamma;\ \Lambda$	Right eigenvectors, left eigenvectors, and eigenvalues of J_R, respectively

Variables

$P_N;\ Z_N$	Number of poles and zeros of the open loop transfer function inside the Nyquist contour
$i_i;\ i_c;\ i_o$	Input, capacitor, and output current of the IBR
N_N	Number of encirclements of the Nyquist plot around $-1 + j0$
P_{IBR}	Power injection of IBRs
$v_i;\ v_o;\ v_g$	IBR's input/output voltages, and grid's Thevenin equivalent voltage, respectively
IF_{ij}	Interaction factor of bus i and bus j
ΔV	Voltage deviation from its rated value
$\theta;\ \omega_s$	Angle and angular frequency of the grid

1. Temporary overvoltage In IBRs Connected Power Systems

1.1 TOV in power grids

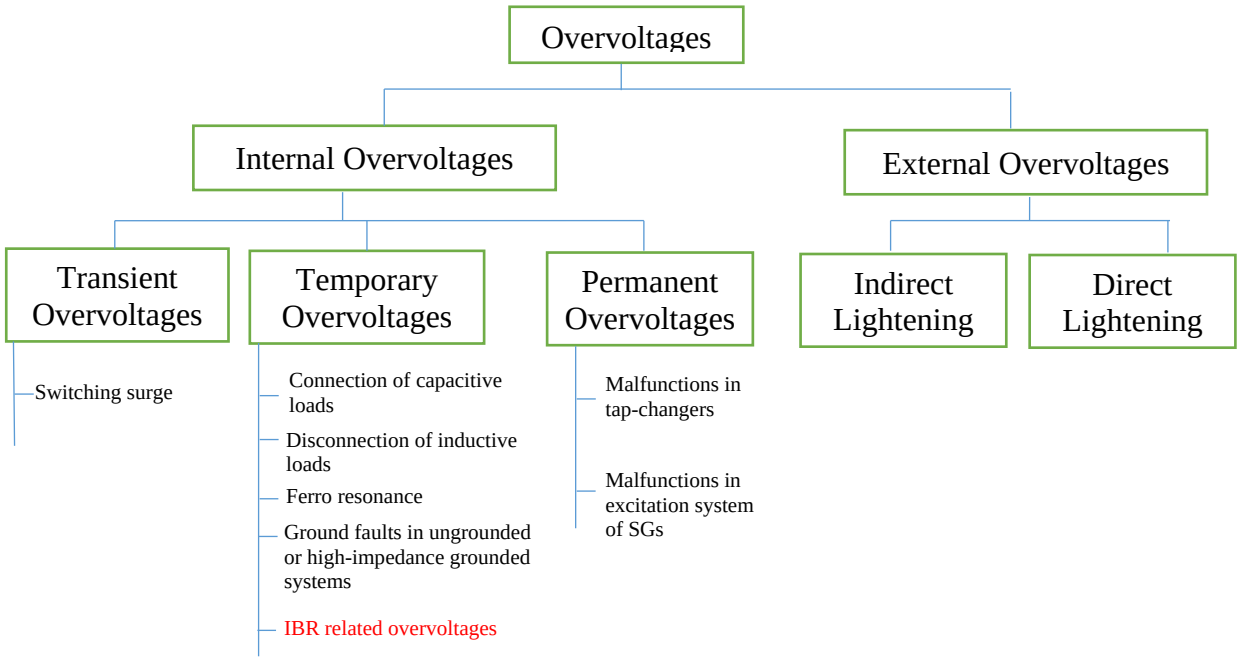

Figure 1-1 Overvoltages in power systems

In general, overvoltages in power systems fall into two main categories: 1) external overvoltages, 2) internal overvoltages. External overvoltages are mainly caused by lightning strikes, either directly or indirectly. Internal overvoltages, on the other hand, stem from numerous sources and fall into three main categories: 1) Transient overvoltages, 2) Temporary overvoltages (TOVs), and 3) Permanent overvoltages. For the case of transient overvoltages, reference [1] defines surges in low voltage grids that last about 50 micro seconds as a transient phenomenon, which are mostly caused by switching actions. On the other hand, TOVs last for much longer periods of time and can cause damage to the equipment. The sources for TOV can be connection of capacitor banks, disconnection of inductive loads, ferro resonance, and IBR related TOVs.

In this project, the focus is studying the TOV phenomenon which occurs immediately after clearing a fault in IBR dominated power grids. This occurs because of excessive reactive power which is built up during faults. For instance [2] evaluates the TOV during the recovery stage of LVRT, due to excessive provision of reactive current after a fault clearance. It is established that the TOV phenomenon is directly correlated with the grid's strength at the point of interconnection (POI). Hence, some efforts have been made to define strength related indices which will effectively highlight the associated risk of TOV.

In the subsequent sections of the report, grid strength indices will be studied, and their strengths and shortcomings will be discussed. Then factors that affect the TOV In IBRs connected systems

will be investigated.

1.2 Grid strength indices

Strength in power grids is the ability to maintain stability in the face of abnormalities. A strong grid has adequate generation capacity and robust control mechanisms to maintain its voltage within the security limit. A strong grid can tolerate faults, detecting, isolating, and resolving them fast enough to prevent cascading failures and outages. On the other hand, a weak grid might go through voltage fluctuations, voltage collapse, and instability during major events, contingencies, and even demand fluctuations. Thus, a weak grid needs to be reinforced with adequate infrastructure and smart control techniques to enhance its response upon contingencies.
In an inverter-based resource (IBR) dominated power grid, the strength of the system should be studied in more detail. IBRs can positively (or negatively) affect the strength of the grid, or a weak grid can disrupt the robust operation of an IBR controller. For instance, when the voltage fluctuates in a weak grid, IBR controllers will not be able to inject sufficient reactive power or adjust the output quickly enough to follow grid's fluctuations, leading to deviations from the setpoint, which eventually leads to loss of synchronism. In addition, it is challenging to comply with grid codes to provide voltage/frequency support when the grid is weak. To provide a deeper understanding of the grid's strength, in the following section various strength indices have been reviewed in detail. Although in essence all the indices try to achieve the same goal, yet each use a different approach and tailored for specific studies.

1.2.1 Short circuit ratio (SCR)

A common criterion to measure the strength is short circuit ratio (SCR). This metric has traditionally been used to refer to the rigidness of the grid's voltage in an area. By calculating the SCR at the point of interconnection (POI) of IBRs, one can identify the weak buses of the system and place and operate the resources accordingly. To compute the SCR, first a three-phase short circuit analysis is conducted at the POI. Then, the ratio between the short-circuit capacity (SCC[1]) and the MW rating of the fault current source at the interconnection bus. In relation to this definition, SCR is as stated below:

$$\mathrm{SCR} = \frac{S_{SC}}{P_R} \tag{1.1}$$

In equation (1.1, S_{SC} is the SCC at the bus in the existing network before the connection of the new generation source, and P_R is the rated MW value of the new connected source [3]. In essence, SCR represents the distance to the voltage boundary limit. Consider equation (1.1. Imagine the goal is to calculate the SCR at bus i of the system. By further simplifying this equation:

$$\mathrm{SCR}_i = \frac{S_{SC\,i}}{P_{R_i}} = \frac{1}{P_{R_i}} \times \frac{|V_i|^2}{|Z_i|} \tag{1.2}$$

[1] Short circuit capacity refers to the maximum current that can flow through a circuit when a short circuit occurs.

Where Z_i is the impedance of the grid at bus i. Based on (1.2, the further away the voltage is from the nominal value, the smaller the SCR, and vice versa.

Though SCR is intuitive, it neglects many aspects contributing to the system's strength. Proximity between plants can result in interactions and oscillations. SCR calculation using Equation (1.2 may yield an overly optimistic result in such scenarios. The high penetration of IBRs inevitably increases the equivalent AC grid impedance, weakening the AC grid and complicating interactions between IBRs and the AC grid. Consequently, the risk of oscillation issues becomes more pronounced in a weakened AC grid. In response to these challenges, many criteria have been introduced in the literature. Various approaches, such as GE's composite SCR (CSCR) and ERCOT's weighted SCR (WSCR) have been suggested to calculate the SCR in weak systems with high concentrations of IBRs. Yet, though many efforts have been made, as of now, there is no well-established standard that considers the IBR interactions in calculating the grid's strength. To get a more accurate estimation of the system strength index and to take interaction effects among producing resources into account, a more reliable indicator that can evaluate the potential risk with complex instabilities is required. In summary, some of the pros and cons of SCR as a measure of grid's strength are as follows:

Pros:

1. Easy and intuitive to obtain with an offline short circuit analysis of the grid.
2. It helps to locate and size various IBRs.

Cons:

1. Missing the dynamics of the system: The short circuit value is a static parameter and does not capture the dynamic behavior of the power system under varying loading conditions. Consequently, IBRs coming from various venders with different controllers have distinct dynamic behaviors during contingencies, which cannot be represented in the generic SCR metric.
2. Does not consider the operating point of the system.
3. Limited to AC Systems: SCR is primarily applicable to AC power systems and may not be directly applicable to DC systems or hybrid AC/DC grids. Therefore, its utility is limited in assessing the strength of emerging grid architectures incorporating DC technologies.

1.2.2 Composite SCR (CSCR)

This approach was first established by GE, with the purpose of evaluating strength while considering IBRs in close (electrical) proximity to the node under examination. CSCR computes the strength without accounting for the fault current contribution, assuming that all converters are connected to a single bus.

By generating a general medium bus voltage, this metric effectively estimates the equivalent system impedance represented by several IBRs.

$$\mathrm{CSCR} = \frac{S_{SC}}{MV_{IBR}} \tag{1.3}$$

In equation (1.3, S_{SC} is the fault level contribution excluding converters and MV_{IBR} is the sum of nominal power ratings of the connected converters. It is easy to identify that creating a median bus and assuming equal contribution from the resources is not accurate since the resources do not have identical behavior and impact on the strength. Although CSCR approximates the strength in

presence of multiple IBRs, this approximation can be inaccurate since the interaction are completely ignored.

Pros and cons of this metric are similar to the conventional SCR. The only difference, as stated, is more accuracy in determining the sources connected to each area, which is captured by defining a median bus as an approximation. In addition, it can be challenging to define the median bus and results will vary with different choices.

1.2.3 Weighted SCR (WSCR)

As previously noted, the standard SCR ignores the interaction among IBRs, even though these units can interact and oscillate as a single unit. In this scenario, conventional SCR would provide a greatly optimistic estimate of the grid's strength.

In addition to CSCR, WSCR is another criterion that attempts to address this problem [4]. Unlike CSCR, WSCR analyzes critical points in the network with IBR linkages by evaluating numerous buses as defined below, where the strength of the complete system is approximated at once.

$$\text{WSCR} = \frac{Weighted\ S_{SC}}{\sum_i^N P_{R,i}} = \frac{\sum_i^N S_{SC,i} \times P_{R,i}}{\left(\sum_i^N P_{R,i}\right)^2} \tag{1.4}$$

In (1.4, $S_{SC,i}$ is the SCC at bus i prior to the connection of the i-th IBR, and $P_{R,i}$ is the nominal power of the i-th IBR to be connected. i is the IBR index, and N is the total number of IBRs that fully interact with one another. WSCR has similar pros and cons which were discussed for SCR, with the following additions:

Pros:

1. Improved generator performance assessment: WSCR provides a more accurate and detailed assessment of a converter's impact on the power system during short circuits compared to the simple SCR. It considers the converter's capacity and impedance in a weighted manner.
2. More comprehensive than SCR: SCR only considers the IBR's apparent power without distinguishing between its active and reactive power contributions. WSCR, by using appropriate weighting factors, considers both real and reactive power components, providing a more comprehensive analysis.

Cons:

1. Although WSCR considers the interaction of IBRs, it does not consider the structure of the grid. In practice, the planners and operators are interested in knowing the strength not only at each IBR POI, but all the other buses as well, which WSCR is incapable of providing those.

1.2.4 Multi-infeed SCR (MISCR)

The CIGRE group [5] developed this metric in an attempt to apply the concept of grid strength to systems with several DC link interconnections. When several converters are connected to the same AC network, the MISCR at a specific bus act as an extension of the SCR and provides a

standardized measurement of the strength of the system at that location, regardless of the number of converters connected.

$$\mathrm{MISCR}_i = \frac{1}{\sum_{j=1}^{K} P_{dc_j}.\, z_{i,j}} \tag{1.5}$$

In equation (1.5, K represents the number of HVdc terminals, P_{dc_j} is the nominal power of the HVdc station j and $z_{i,j}$ is ij-th element in Z_{BUS} of the network. According to the definition of Z_{BUS}, the element in the i-th row and j-th column shows bus i's sensitivity to load fluctuations in bus j. A larger value for this term indicates that converter j has a greater impact on converter i.

Pros:

1. Considering the interaction between the sources.

Cons:

1. Ignoring the dynamics of the system.
2. Does not consider the operating point of the system.

1.2.5 Multi-infeed effective SCR (MESCR)

MESCR considers the interaction of DC rectifiers by defining a multi-infeed interaction factor (MIIF) as in (1.6,

$$\mathrm{MIIF}_{ij} = \frac{U_i}{U_j} = \left|\frac{z_{ij}}{z_{jj}}\right| \tag{1.6}$$

where U_i and U_j represent the rated voltages of the i-th and j-th commutation buses. Z_{ij} represents the mutual impedance between the i-th and j-th buses, while z_{jj} is the impedance matrix denotes the self-impedance at the j-th bus. Once all the interaction factors are calculated, a matrix is formed where the diagonal elements, which represent the self-interaction, are equal to one. The rest of the elements vary between zero and one, where values closer to one indicate stronger interactions and those closer to zero indicate looser interactions. Based on (1.6, MIIF_{ij} and MIIF_{ji} are not necessarily equal and the resulting matrix can be non-symmetric.

To develop the concept of MESCR, first we discuss the derivation of Effective SCR (ESCR). The conventional definition of a single infeed inverter bus is as follows:

$$\mathrm{ESCR}_i = \frac{S_{SC,i} - Q_{c,i}}{P_{dc,i}} \tag{1.7}$$

In (1.7, $S_{SC,i}$ is the three phase SCC of the AC system of the i-th DC commutation bus, $Q_{C,i}$ denotes the reactive power shunt compensation, and $P_{dc,i}$ and $Q_{dc,i}$ are the power of DC i and j, respectively. Then, by redefining the value of $P_{dc,i}$ to consider the effect of the interaction factors, MESCR is defined as follows:

$$\text{MESCR}_i = \frac{S_{SC,i} - Q_{c,i}}{P_{dc,i} + \sum_{j=1,j\neq i}^{k} MIIF_{ij} \times P_{dc,j}} \quad (1.8)$$

The pros and cons are similar to MISCR, the difference being that the rated conditions of the voltages contribute to the strength measure.

1.2.6 Inverter interaction level SCR (IILSCR)

IILSCR is a dynamic strength measure that takes into account the online real power contribution of the neighboring IBRs. To do so, a power flow tracing algorithm is required to decompose the share of each IBR injected to the bus i under study. This way, it is not necessary to determine the boundaries from which the IBRs within an area oscillate with one another. In equation (1.9 below:

$$\text{IILSCR}_i = \frac{S_{SC,i}}{P_{IBR,i} + \sum_{m=1,m\neq i}^{N} P_{IBR,(m-i)}} \quad (1.9)$$

$S_{SC,i}$ is the SCC of bus i, $P_{IBR,i}$ is the power rating of IBR installed on bus i, $P_{IBR,(m-i)}$ is power injection from neighboring IBRs. IILSCR relies heavily on power flow studies, which entails the following pros and cons:

Pros:

1. IILSCR leverages a comprehensive understanding of the flow of power within the system under various operating conditions, which results in measuring the interactions in a dynamic and accurate fashion.

Cons:

1. Complexity: Power flow analysis can be computationally demanding, particularly in large-scale power systems with several linked grids. Performing detailed analyses may require significant computational resources and time.
2. Modeling assumptions: power flow analysis relies on various modeling assumptions, such as the representation of system components, load characteristics, and generation dispatch, line limits, etc. Inaccurate or unrealistic assumptions can lead to unreliable results and misinterpretation of the system's strength.

1.2.7 Site dependent SCR (SDSCR)

The concept underlying SDSCR is to measure the impacts of several IBR interactions that are installed on distinct buses separately [6]. The physical distance between the IBRs is modelled by considering the impedance of the lines. To begin with, first the network model is partitioned into two parts: 1) buses including conventional generators, 2) buses including IBRs, as depicted in (1.10:

$$\begin{bmatrix} V_G \\ V_R \end{bmatrix} = \begin{bmatrix} Z_{GG} & Z_{GR} \\ Z_{RG} & Z_{RR} \end{bmatrix} \begin{bmatrix} I_G \\ I_R \end{bmatrix} \quad (1.10)$$

Where V_G and I_G are vectors of voltages and currents containing the synchronous generators, and V_R and I_R represent the buses containing the IBRs. Once these voltages are obtained, the SDSCR at each bus is calculated as follows:

$$\mathrm{SDSCR}_i = \frac{|V_{R,i}|^2}{\left(P_{R,i} + \sum_{j \in R, j \neq i}^{N} P_{R,j} w_{ij}\right)|Z_{RR,ii}|} \tag{1.11}$$

where each weight is calculated as follows:

$$w_{ij} = \frac{Z_{RR,ij}}{Z_{RR,ii}} \left(\frac{V_{R,i}}{V_{R,j}}\right)^* \tag{1.12}$$

In equation (1.12, IBR interactions are taken into account considering the physical location of the neighboring IBRs. This means that to measure the strength at bus i, first the power injection $P_{R,i}$ from the respective IBR at that bus is considered. Next, this term is complemented with the contributions from the neighboring IBRs, $P_{R,j}$, each scaled by the voltages and impedances to the reflect not only the physical distance between the IBRs but also the distance to voltage boundary limit. In addition, all the term in the denominator is also scaled to the self-impedance of the bus i, $Z_{RR,ii}$. This way, if the IBRs on buses i and j are in close proximity, $Z_{RR,ii} \approx Z_{RR,ij}$, and the coupling impact of j on i will increase.

Comparing (1.11 with (1.2, it is evident that SDSCR is a more comprehensive version of the traditional SCR. When there is only one IBR on bus i and no IBR on neighboring buses, (1.11 will be the same as 1.2. this also indicates that both SCR and SDSCR measure the distance to the voltage boundary limit implicitly and explicitly, respectively. This also means that the same ranges that indicate a weak grid in SCR will roughly be applicable to SDSCR, indicating that a weak grid is essentially operating close to the volage stability boundary.

Pros:

1. the dynamics of voltages, power flow, as well as the grid structure are accounted for in measuring the strength of each node.

Cons:

1. computational burden of conducting the power flows, which are a function of the grid's operating conditions, making it challenging to calculate the worst case.

1.2.8 SCR with interaction factors (SCRIF)

To capture the effect of voltage deviations, the WSCR can be augmented with an interaction factor $\mathrm{IF}_{ij} = \frac{\Delta V_i}{\Delta V_j}$ as follows:

$$\mathrm{SCRIF}_i = \frac{S_{SC,i}}{P_{IBR,i} + \sum_{j=1, j \neq i}^{N} \mathrm{IF}_{ij} \times P_{IBR,j}} \tag{1.13}$$

Subscript j in this equation denotes all nearby buses that are electrically close to IBRs, or other buses. The coupling interaction of bus j on bus i is denoted by IF_{ij}. The voltage deviations at the

i-th and j-th bus, respectively, are represented by ΔV_i and ΔV_j. The nominal power rating and SCC contribution at bus i are denoted by $P_{IBR,i}$ and $S_{SC,i}$, respectively. Based on this derivation, when the voltage is stiffer, the interaction would be less, and the SCRIF would be a higher value.

1.2.9 Equivalent SCR (ESCR)

Equivalent circuit-based SCR (ESCR) was first proposed by CIGRE group in [7] to address the interactions of adjacent or electrically close wind power plants in measuring the system's strength. To begin with, assume a grid connected IBR. This system can be further simplified as depicted in Figure 1-2, where Z_g is the impedance in which R_g and L_g represent the impedance of the grid, and L_f, R_f, and C_f are the impedance of the IBR filter.

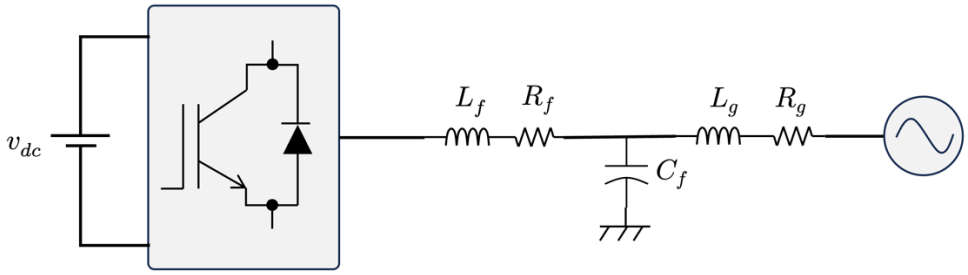

Figure 1-2 Schematic of a generic grid connected IBR

As discussed before, at the POI, the SCR of the system can be defined as in equation (1.14. Assuming that the base value of the system is P_{IBR}, this equation is further simplified in the p.u. system as follows:

$$S_{SC,PU} = \frac{v_{POI,PU}^2}{Z_{sys,PU}} = \frac{1}{Z_{sys,PU}} \tag{1.14}$$

Where $Z_{sys,PU}$ is the network impedance at the POI, and $v_{POI,PU}$ is the voltage, all in the per unit system. Substituting (1.14 in (1.16 gives:

$$\mathrm{ESCR}_{POI} = \frac{1}{Z_{sys,PU}} \tag{1.15}$$

Based on this simplification, SCR at POI is the inverse of the impedance observed at POI. This is consistent with the definition of SCR, as higher impedance indicates a weak grid and vice versa.
To generalize this concept to multi-infeed systems, similar approaches as SCRIF has been utilized. Once again consider the interaction factor is defined as $\mathrm{IF}_{ij} = \frac{\Delta V_i}{\Delta V_j}$, where ΔV_i is a small voltage deviation on bus i resulting from a small voltage change on bus j. The closer IBR j is to IBR i, the bigger the interaction factor will be. For IBRs that are far away from each other, IF_{ij} will be negligible and if both i and j are on the same bus, this coefficient will be unity. To understand the coupling effect of multi-infeed power systems, when several IBRs are electrically close to each other, they share the SCC of the grid. Consequently, the SCR calculated from the perspective of the IBR will be higher than the actual value. With this generalization, the following equation is utilized to calculate the ESCR in multi-infeed systems:

$$\mathrm{ESCR}_i = \frac{S_{SC,i}}{P_{R,i} + \sum_j \mathrm{IF}_{ji} \times P_{R,j}} \tag{1.16}$$

Similar to the single infeed definition, ESCR can be further simplified in per unit system to be applicable to any network configuration as follows. Consider equation (1.17 which depicts the relationship between the node voltages and branch currents in a given network.

$$\begin{pmatrix} V_1 \\ V_2 \\ \vdots \\ V_n \end{pmatrix} = Z_{bus} \begin{pmatrix} I_1 \\ I_2 \\ \vdots \\ I_m \end{pmatrix} \tag{1.17}$$

Assuming a small change in the current at i-th node, the respective voltage changes on nodes i and j will be calculated as follows:

$$\begin{aligned} \Delta V_j &= z_{ji} \Delta I_i \\ \Delta V_i &= z_{ii} \Delta I_i \end{aligned} \tag{1.18}$$

Given this simplification, the impact factor is further simplified as:

$$IF_{ji} = \frac{\Delta V_j}{\Delta V_i} = \frac{z_{ji}}{z_{ii}} \tag{1.19}$$

Also, assuming the power of the IBR to be connected is the base value of the system:

$$SCR_i = \frac{S_{SC,i}}{P_{R,i}} = \frac{1}{Z_{ii}} \tag{1.20}$$

With this assumption, the formula in (1.15 is further simplified as:

$$\begin{aligned} ESCR_i = \frac{S_{SC,i}}{P_{R,i} + \sum_j IF_{ji} \times P_{R,j}} &= \frac{P_{R,i}/z_{ii}}{P_{R,i} + \sum_{j=1,m,j\neq i} \frac{z_{ji}}{z_{ii}} \times P_{R,j}} \\ &= \frac{1}{\sum_{j=1,m} z_{ji} \times P_{R,j,PU}} \end{aligned} \tag{1.21}$$

The metric provides an upper limit on the network impedance that the converter can function with. Note that this model does not account for how the output impedance is affected by the IBR controller system.

1.2.10 Grid strength impedance metric (GSIM)

In all of the previous methods, the interaction factors disregarded the control system of the IBR, assuming identical control behavior. In reality, IBRs coming from various vendors behave differently from one another. To address this issue, a method devised in [8] considers the MIMO

impedance behavior of the IBR to estimate the strength of the entire system. By using this method, it is possible to model every component of the IBR in extensive detail, and as a result, this criterion assesses the strength across any given frequency spectrum. Consider the small-signal output admittance, represented in the synchronous reference frame of either the grid-forming or grid-following IBR as shown in equation (1.22:

$$Y_{vsc} = \frac{\Delta i}{\Delta v} = \begin{bmatrix} Y_{qq,c} & Y_{qd,c} \\ Y_{dq,c} & Y_{dd,c} \end{bmatrix} \tag{1.22}$$

Then, the base impedance of the grid is calculated as in equation (1.23:

$$Z_b = \begin{bmatrix} R_b + sL_b & \omega_b L_b \\ -\omega_b L_b & R_b + sL_b \end{bmatrix} \tag{1.23}$$

In which $R_b = Z_b \frac{R}{X}$ and $L_b = \frac{Z_b}{\omega_b}$, where Z_b is the base impedance of the system, ω_b is the fundamental frequency, and $\frac{R}{X}$ is the desired ratio of resistance to reactance of the network. This approach has the advantage that the impedances can be obtained by sweeping over the frequency spectrum in system identification techniques, negating the need for extensive modeling. In the following, $Y_{sys}(s)$ is the admittance of the system under study, and Z_b is the base value for the impedance.

$$Y_{sys}(s) = \begin{bmatrix} Y_{qq}(s) & Y_{qd}(s) \\ Y_{dq}(s) & Y_{dd}(s) \end{bmatrix} \tag{1.24}$$

$$Z_b = \begin{bmatrix} Z_{qq}(s) & Z_{qd}(s) \\ Z_{dq}(s) & Z_{dd}(s) \end{bmatrix} \tag{1.25}$$

Each of the 2×2 matrices then produce two eigenloci denoted q and d. by elementwise multiplication of the eigenvalues, the GSIM metric is developed as follows:

$$\begin{bmatrix} \mathrm{GSIM}_d(s) \\ \mathrm{GSIM}_q(s) \end{bmatrix} = \lambda(Y_{sys}(s)) \odot \lambda(Z_b(s)) \tag{1.26}$$

Combining the two components together to take into account the interaction between the two axes yields the following result:

$$\mathrm{GSIM}(s) = \sqrt{\frac{\mathrm{GSIM}_d^2(s) + \mathrm{GSIM}_q^2(s)}{2}} \tag{1.27}$$

This measure effectively estimates the strength in a wide range of frequency for which the linearized impedance is valid. The catch is that modelling each IBR controller based on various control techniques can a challenging task. With just a few numbers of IBRs, the model can easily become intractable.

1.2.11 QV modal analysis

This method relies on the Jacobian matrix of the system to develop a strength measure. The Jacobian has the following format [9]:

$$\begin{bmatrix}\Delta P\\ \Delta Q\end{bmatrix} = \begin{bmatrix}J_{11} & J_{12}\\ J_{21} & J_{22}\end{bmatrix}\begin{bmatrix}\Delta\theta\\ \Delta V\end{bmatrix} \tag{1.28}$$

In this equation, ΔP and ΔQ represent active power and reactive power mismatches, respectively, and ΔV represents unknown voltage magnitude, and $\Delta\theta$ indicates angle correction. In power grids, ΔP and ΔQ are weakly coupled in most operating scenarios. Assuming $\Delta P = 0$, the above equation can be further simplified as follows:

$$\Delta Q = J_R \Delta V \tag{1.29}$$

$$\Delta V = J_R^{-1}\Delta Q \tag{1.30}$$

Where J_R is the reduced Jacobian:

$$J_R = [J_{22} - J_{21}\, J_{11}^{-1}\, J_{12}] \tag{1.31}$$

The eigenvector of the reduced Jacobian can reveal the weak nodes in the power system under study, while the size of the Jacobian matrix's eigenvalues can predict the static voltage boundary margin of a particular bus. Using eigenvalues and eigenvectors, the reduced Jacobian can be broken down as follows:

$$J_R = \Phi \Lambda^{-1} \Gamma \tag{1.32}$$

Where Φ is the right eigenvector of J_R, Γ is the diagonal eigenvalue matrix, and Λ is the left eigenvalue matrix of J_R. By inputting this decomposition into the reduced QV equation:

$$\Delta V = \sum_{i=1}^{n} \frac{\Phi_i \Gamma_i}{\lambda_i} \Delta Q \tag{1.33}$$

Equation (1.33 contains the information regarding the weakest nodes in the grid. In this equation, λ_i is the eigenvalue of J_R, Φ_i is its right eigenvalue, and Γ_i is the mode. This is a dynamic model that can track the system strength based on various conditions. Although a simplified average model of IBR is required to calculate the power flow results, hence the controller dynamics are ignored.

1.2.12 Generalized SCR (gSCR)

The SCR metric was developed to estimate the strength of single-infeed integration of IBRs. Next, various metrics were discussed that tried to deal with the multi-infeed systems. Among these techniques, those which develop a strength measure using linearized power flow equations with

reduced Jacobian matrix fall in a category called generalized SCR (gSCR). This concept is close to that off SDSCR, where it begins by further simplifying the SCR definition as shown in (1.2 to demonstrate how the definition of SCR is implicitly tied to the distance to the static voltage boundary limits, and then trying to extend that to a network with multiple IBRs. For instance, the gSCR metric developed in [10] utilizes eigenvalue decomposition from a voltage stability perspective, through the linearization of AC power flow equations. The minimal eigenvalue of the system's extended admittance matrix is referred to as gSCR. For instance, in a multi-infeed DC transmission system:

$$\mathrm{gSCR} = \min \lambda(J_B) \tag{1.34}$$

In which J_B is the extended admittance matrix of the multi-infeed network, defined as:

$$J_B = \begin{pmatrix} P_1 & \cdots & 0 \\ \vdots & \ddots & \vdots \\ 0 & \cdots & P_n \end{pmatrix}^{-1} \begin{pmatrix} B_{11} & \cdots & B_{1n} \\ \vdots & \ddots & \vdots \\ B_{n1} & \cdots & B_{nn} \end{pmatrix} \tag{1.35}$$

In this equation, P_i is the admittance matrix of the i-th DC interconnection, and B_{ii} and B_{ij} are the imaginary parts of the elements in the AC system equivalent admittance matrix at the DC infeed buses. Based on the case studies demonstrated in [10], when the gSCR is less than two at an DC infeed bus, it indicates that this interconnection is weak and is susceptible to voltage oscillations. But for gSCR values greater than 3, the AC system is robust enough to host the HVdc system, ensuring that the limit operating condition of the HVdc system is guaranteed in normal operating conditions.

1.2.13 Summary and comparison of strength indices

In this report, methods that can be utilized to measure the strength of the power grid were briefly explained. It starts with the SCR, which is well established for analyzing grid's strength. SCR does not consider the network's structure, coupling among the resources, which causes interactions and oscillations, and dynamics of the IBR controllers. To resolve these shortcomings, various approaches were reviewed which tried to incorporate the grid's structure, by assigning weights to adjacent contributing IBRs, and the voltage boundary limits. SCR only assumes the units connected to the node under study, CSCR assumes a single bus where all IBRs are connected to, and contribute equally, WSCR is similar to CSCR, but assumes multiple points in the system, and SCRIF captures voltage deviations among the bus under study and the adjacent contributing buses. Most of these methods ignore the dynamics of IBRs, and only consider the strength in fundamental frequency. Another shortcoming of these methods is that the fault behavior of IBRs is not identical to the behavior of conventional generators, based on which most of these methods are developed. To address these challenges, an impedance-based category of criteria has been introduced that do not necessarily consider quasi-steady state operation of IBRs, such as GSIM. Another advantage of this technique is that the two different control techniques of IBRs, namely grid following and grid forming, could be applied to assess which of them would increase the system's strength at each POI.

1.3 Factors affecting the temporary overvoltages in IBRs connected systems

In this project we investigated different factors that may affect the temporary overvoltages. The case study results showed that the reduction in the strength of the system that may lead to grid synchronization Instability and delays in the protection logics of IBRs (i.e. fault ride through logic) are influential factors. In the subsequent sections the impacts of above factors are studied analytically based on the state space and impedance-based methods and numerically based on time domain simulations.

1.4 State space model

Assume there is a grid-tied inverter as depicted in Figure 1-3. The inverter is interfaced with the AC grid through an LC filter. A phase locked loop (PLL) is implemented to measure the voltage angle and the frequency of the grid.

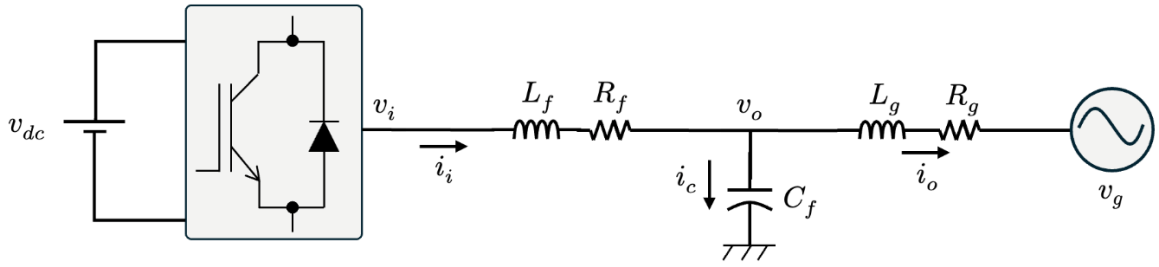

Figure 1-3 Grid-tied IBR system

To begin with, by writing the KVL at the filter, the following equation is obtained:

$$\begin{bmatrix} v_{ia} \\ v_{ib} \\ v_{ic} \end{bmatrix} - \begin{bmatrix} v_{oa} \\ v_{ob} \\ v_{oc} \end{bmatrix} = R_f \begin{bmatrix} i_{ia} \\ i_{ib} \\ i_{ic} \end{bmatrix} + L_f \frac{d}{dt} \begin{bmatrix} i_{ia} \\ i_{ib} \\ i_{ic} \end{bmatrix} \tag{1.36}$$

Using the Park transform in (1.37, any 3-phase signal can be transformed to dc signals in dq frame, where it is much more convenient to work with dc signals.

$$\begin{bmatrix} x_d \\ x_q \\ x_0 \end{bmatrix} = \underbrace{\sqrt{\frac{2}{3}} \begin{bmatrix} cos\,(\theta) & cos\,(\theta - \frac{2\pi}{3}) & cos\,(\theta + \frac{2\pi}{3}) \\ -sin\,(\theta) & -sin\,(\theta - \frac{2\pi}{3}) & -sin\,(\theta + \frac{2\pi}{3}) \\ \frac{1}{\sqrt{2}} & \frac{1}{\sqrt{2}} & \frac{1}{\sqrt{2}} \end{bmatrix}}_{\mathbf{T}_{dq}} \begin{bmatrix} x_a \\ x_b \\ x_c \end{bmatrix} \tag{1.37}$$

In this equation, x_{abc} and x_{dq0} are arbitrary signals in abc and dq frames, respectively, and $\theta = \omega_s t$, where ω_s represents the synchronous speed at which the dq frame rotates. By multiplying

the inverse of $\mathbf{T}_{dq}$ to the both sides of (1.36 and further simplifying the results, equations (1.38 and (1.39 called the two-axis equation of the IBR are obtained.

$$\frac{di_{id}}{dt} = \frac{1}{L_f}(v_{id} - R_f i_{id} + \omega_s L_f i_{iq} - v_{od}) \tag{1.38}$$

$$\frac{di_{iq}}{dt} = \frac{1}{L_f}(v_{iq} - R_f i_{iq} - \omega_s L_f i_{id} - v_{oq}) \tag{1.39}$$

The current controller is depicted in Figure 1-5. The objective of this controller is to generate proper voltage modulation signals for which the current references are tracked. In addition, assuming the PLL effect, the signals in the controller frame deviate from the signals in the grid frame as depicted in Figure 1-4, and to differentiate between the two, those in the control frame are denoted with the superscript c.

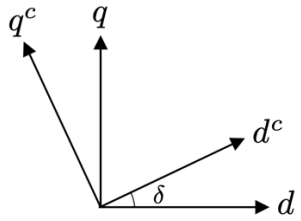

Figure 1-4 angle deviation between the grid and the controller frames

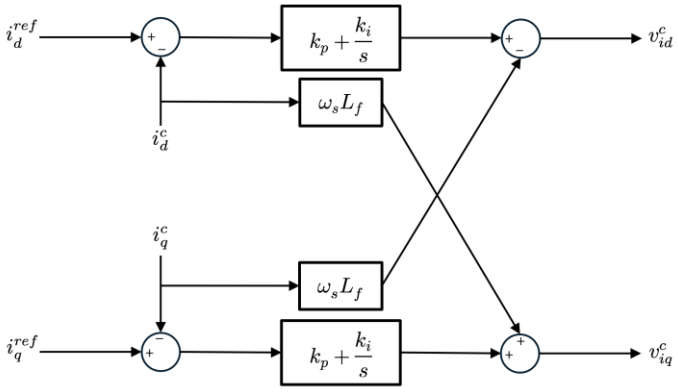

Figure 1-5 Two-axis current controller

By writing the equation of each channel separately, the output voltages are obtained as follows:

$$v_{id}^c = -\omega_s L_f i_{iq}^c + k_p\left(i_{id}^{ref} - i_{id}^c\right) + k_i \int \left(i_{id}^{ref} - i_{id}^c\right) dt \tag{1.40}$$

$$v_{iq}^c = \omega_s L_f i_{id}^c + k_p\left(i_{iq}^{ref} - i_{iq}^c\right) + k_i \int \left(i_{iq}^{ref} - i_{iq}^c\right) dt \tag{1.41}$$

Next, the PLL is implemented for the IBR to track the angle and the frequency of the grid. The controller block diagram of the PLL is depicted in Figure 1-6.

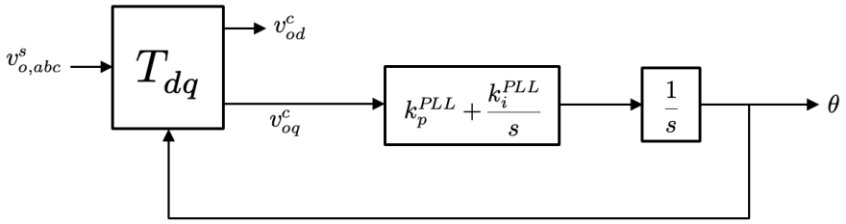

Figure 1-6 Synchronous reference frame PLL

which gives the following equation:

$$\Delta\theta = (k_p^{PLL}\Delta v_{oq}^c + k_i^{PLL}\int \Delta v_{oq}^c dt)\frac{1}{s} \tag{1.42}$$

The addition of PLL creates nonlinearity in the state equations. To develop the state space model, the linearized dynamics of the PLL are considered as follows.

$$\Delta\psi = \int \Delta v_{oq}^c dt \tag{1.43}$$

$$\frac{d}{dt}\begin{bmatrix}\Delta\theta\\ \Delta\psi\end{bmatrix} = \begin{bmatrix}0 & k_i^{PLL}\\ 0 & 0\end{bmatrix}\begin{bmatrix}\Delta\theta\\ \Delta\psi\end{bmatrix} + \begin{bmatrix}0 & k_p^{PLL}\\ 0 & 1\end{bmatrix}\begin{bmatrix}\Delta v_{od}^c\\ \Delta v_{oq}^c\end{bmatrix} \tag{1.44}$$

In equations (1.40, (1.41, and (1.44, signals are in the control frame. In the final state equations, all the signals should be on the same frame. In steady state, the angle δ is zero, which means that the two frames are aligned and the PLL is perfectly tracking the grid's angle and frequency. Once a small disturbance occurs, this propagates to the IBR through the PLL dynamics, for which there will be an angular difference for the grid's synchronous frame (denoted by s) and the IBR's control frame (denoted by c). The capital letters represent steady state values of the voltages and currents:

$$\begin{bmatrix}V_{id}^c\\ V_{iq}^c\end{bmatrix} = \begin{bmatrix}V_{id}^s\\ V_{iq}^s\end{bmatrix};\ \begin{bmatrix}V_{od}^c\\ V_{oq}^s\end{bmatrix} = \begin{bmatrix}V_{od}^s\\ V_{oq}^s\end{bmatrix};\ \begin{bmatrix}I_{id}^c\\ I_{iq}^c\end{bmatrix} = \begin{bmatrix}I_{id}^s\\ I_{iq}^s\end{bmatrix};\ \begin{bmatrix}I_{od}^c\\ I_{oq}^c\end{bmatrix} = \begin{bmatrix}I_{od}^s\\ I_{oq}^s\end{bmatrix} \tag{1.45}$$

Since these steady state values are equal, the superscripts are dropped, and capital letters indicate steady state values. Assuming a small disturbance in the angular frequency $\Delta\theta \approx 0$:

$$T_{\Delta\theta} = \begin{bmatrix}\cos(\Delta\theta) & \sin(\Delta\theta)\\ -\sin(\Delta\theta) & \cos(\Delta\theta)\end{bmatrix} = \begin{bmatrix}1 & \Delta\theta\\ -\Delta\theta & 1\end{bmatrix} \tag{1.46}$$

Using this transformation, the relationship between the signals in the system frame and the control frame is linearized as follows. For the output voltage:

$$\begin{bmatrix} V_{od} + \Delta v_{od}^{c} \\ V_{oq} + \Delta v_{oq}^{c} \end{bmatrix} = \begin{bmatrix} 1 & \theta \\ -\theta & 1 \end{bmatrix} \begin{bmatrix} V_{od} + \Delta v_{od}^{s} \\ V_{oq} + \Delta v_{oq}^{s} \end{bmatrix} \tag{1.47}$$

$$\begin{bmatrix} \Delta v_{od}^{c} \\ \Delta v_{oq}^{c} \end{bmatrix} \approx \begin{bmatrix} \Delta v_{od}^{s} + V_{oq}\Delta\theta \\ \Delta v_{oq}^{s} - V_{od}\Delta\theta \end{bmatrix}$$

And for the input voltage and current:

$$\begin{bmatrix} I_{id} + \Delta i_{id}^{c} \\ I_{iq} + \Delta i_{iq}^{c} \end{bmatrix} = \begin{bmatrix} 1 & \theta \\ -\theta & 1 \end{bmatrix} \begin{bmatrix} I_{id} + \Delta i_{id}^{s} \\ I_{iq} + \Delta i_{iq}^{s} \end{bmatrix} \tag{1.48}$$

$$\begin{bmatrix} V_{id} + \Delta v_{id}^{s} \\ V_{iq} + \Delta v_{iq}^{s} \end{bmatrix} = \begin{bmatrix} 1 & \theta \\ -\theta & 1 \end{bmatrix}^{-1} \begin{bmatrix} V_{id} + \Delta v_{od}^{c} \\ V_{iq} + \Delta v_{oq}^{c} \end{bmatrix} \tag{1.49}$$

Using the transformation in (1.47, the state equations of the PLL in (1.44 are transformed to the system's frame as follows:

$$\frac{d}{dt}\begin{bmatrix} \Delta\theta \\ \Delta\psi \end{bmatrix} = \begin{bmatrix} -k_p^{PLL} V_{od}^{s} & k_i^{PLL} \\ -V_{od}^{s} & 0 \end{bmatrix} \begin{bmatrix} \Delta\theta \\ \Delta\psi \end{bmatrix} + \begin{bmatrix} 0 & k_p^{PLL} \\ 0 & 1 \end{bmatrix} \begin{bmatrix} \Delta v_{od}^{s} \\ \Delta v_{oq}^{s} \end{bmatrix} \tag{1.50}$$

Next, the two axis controller equations are unified to the same frame. First, the following states are introduced to consider the integral action in the PI controller:

$$\Delta\gamma_d = \int \left(\Delta i_d^{ref} - \Delta i_d^{c}\right) dt \tag{1.51}$$

$$\Delta\dot{\gamma}_d = \Delta i_d^{ref} - \left(\Delta i_d^{s} + \Delta\theta I_q^{s}\right) \tag{1.52}$$

$$\Delta\gamma_q = \int \left(\Delta i_q^{ref} - \Delta i_q^{c}\right) dt \tag{1.53}$$

$$\Delta\dot{\gamma}_q = \Delta i_q^{ref} - \left(\Delta i_q^{s} - \Delta\theta I_d^{s}\right) \tag{1.54}$$

By inputting these linearized values into (1.40 and (1.41, the following equations are obtained:

$$\Delta v_{id}^{s} + V_{iq}\Delta\theta = -\omega_s L_f\left(\Delta i_{iq}^{s} - I_{id}\Delta\theta\right) + k_p\left(\Delta i_{id}^{ref} - \left(\Delta i_{id}^{s} + I_{iq}\Delta\theta\right)\right) + k_i\Delta\gamma_d \tag{1.55}$$

$$\Delta v_{iq}^{s} - V_{id}\Delta\theta = \omega_s L_f\left(\Delta i_{id}^{s} + I_{iq}\Delta\theta\right) + k_p\left(\Delta i_{iq}^{ref} - \left(\Delta i_{iq}^{s} - I_{id}\Delta\theta\right)\right) + k_i\Delta\gamma_q \tag{1.56}$$

By further simplifying these equations:

$$\Delta v_{id}^{s} = \left(-V_{iq} + \omega_s L_f I_{id} - k_p I_{iq}\right)\Delta\theta + k_p\Delta i_{id}^{ref} - k_p\Delta i_{id}^{s} - \omega_s L_f\Delta i_{iq}^{s} + k_i\Delta\gamma_d \tag{1.57}$$

$$\Delta v_{iq}^{s} = \left(V_{id} + \omega_s L_f I_{iq} - k_p I_{id}\right)\Delta\theta + k_p \Delta i_{iq}^{ref} - k_p \Delta i_{iq}^{s} + \omega_s L_f \Delta i_{id}^{s} + k_i \Delta\gamma_q \quad (1.58)$$

By inputting these voltage signals into (1.38 and (1.39:

$$\frac{d\Delta i_{id}^{s}}{dt} = \frac{1}{L_f}\Big(\left(-V_{iq}^{s} + \omega_s L_f I_{id}^{s} - k_p I_{iq}^{s}\right)\Delta\theta + k_p \Delta i_{id}^{ref} - \left(k_p + R_f\right)\Delta i_{id}^{s} + k_i \Delta\gamma_d - \Delta v_{od}^{s}\Big) \quad (1.59)$$

$$\frac{d\Delta i_{iq}^{s}}{dt} = \frac{1}{L_f}\Big(\left(V_{id}^{s} + \omega_s L_f I_{iq}^{s} + k_p I_{id}^{s}\right)\Delta\theta + k_p \Delta i_{iq}^{ref} - \left(k_p + R_f\right)\Delta i_{iq}^{s} + k_i \Delta\gamma_q - \Delta v_{oq}^{s}\Big) \quad (1.60)$$

Next, the dynamics of the filter's capacitor are introduced by writing a KCL at POI as follows:

$$\boldsymbol{T}_{dq}^{-1} \times \frac{d}{dt}\begin{bmatrix}\Delta v_{oa}^{s}\\ \Delta v_{ob}^{s}\\ \Delta v_{oc}^{s}\end{bmatrix} = \frac{1}{C_f} \times \boldsymbol{T}_{dq}^{-1} \times \left(\begin{bmatrix}\Delta i_{ia}^{s}\\ \Delta i_{ib}^{s}\\ \Delta i_{ic}^{s}\end{bmatrix} - \begin{bmatrix}\Delta i_{oa}^{s}\\ \Delta i_{ob}^{s}\\ \Delta i_{oc}^{s}\end{bmatrix}\right) \quad (1.61)$$

By transforming this into the dq frame, the following dynamics are obtained:

$$\frac{d\Delta v_{od}^{s}}{dt} = \frac{1}{C_f}\left(\Delta i_{id}^{s} + \omega_s C_f \Delta v_{oq}^{s} - \Delta i_{od}^{s}\right) \quad (1.62)$$

$$\frac{d\Delta v_{oq}^{s}}{dt} = \frac{1}{C_f}\left(\Delta i_{iq}^{s} - \omega_s C_f \Delta v_{od}^{s} - \Delta i_{oq}^{s}\right) \quad (1.63)$$

Finally, the dynamics of the grid are added as follows:

$$\begin{bmatrix}\Delta v_{oa}\\ \Delta v_{ob}\\ \Delta v_{oc}\end{bmatrix} - \begin{bmatrix}\Delta v_{ga}\\ \Delta v_{gb}\\ \Delta v_{gc}\end{bmatrix} = R_g \begin{bmatrix}\Delta i_{oa}\\ \Delta i_{ob}\\ \Delta i_{oc}\end{bmatrix} + L_g \frac{d}{dt}\begin{bmatrix}\Delta i_{oa}\\ \Delta i_{ob}\\ \Delta i_{oc}\end{bmatrix} \quad (1.64)$$

Transforming (1.64 to the dq frame, the two axis grid dynamics equations are obtained as in (1.65 and (1.66:

$$\frac{d\Delta i_{gd}^{s}}{dt} = \frac{1}{L_g}\left(\Delta v_{od}^{s} - R_g \Delta i_{gd}^{s} - \omega_s L_g \Delta i_{gq}^{s} - \Delta v_{gd}^{s}\right) \quad (1.65)$$

$$\frac{d\Delta i_{gq}^{s}}{dt} = \frac{1}{L_g}\left(\Delta v_{oq}^{s} - R_g \Delta i_{gq}^{s} - \omega_s L_g \Delta i_{gd}^{s} - \Delta v_{gq}^{s}\right) \quad (1.66)$$

In the system developed above, the state vector X, the input vector u, and the output vector y are depicted in (1.67.

$$X = [\Delta i_{id}^s, \Delta i_{iq}^s, \Delta i_{od}^s, \Delta i_{oq}^s, \Delta v_{od}^s, \Delta v_{oq}^s, \Delta\theta, \Delta\psi, \Delta\gamma_d, \Delta\gamma_q]$$
$$u = [\Delta i_{id}^{ref}, \Delta i_{iq}^{ref}, \Delta v_{gd}^s, \Delta v_{gq}^s] \quad (1.67)$$
$$y = [\Delta i_{id}^s, \Delta i_{iq}^s, \Delta v_{od}^s, \Delta v_{oq}^s]$$

Where $\dot{X} = AX + Bu$ and $y = CX$, and matrices A, B, and C are as follows:

$$A = \begin{bmatrix} -\frac{k_p+R_f}{L_f} & 0 & 0 & 0 & -1 & 0 & \frac{-V_{iq}+\omega_s L_f I_{id}-k_p I_{iq}}{L_f} & 0 & \frac{k_i}{L_f} & 0 \\ 0 & -\frac{k_p+R_f}{L_f} & 0 & 0 & 0 & -1 & \frac{V_{id}+\omega_s L_f I_{iq}-k_p I_{id}}{L_f} & 0 & 0 & \frac{k_i}{L_f} \\ 0 & 0 & -\frac{R_g}{L_g} & \omega_s & \frac{1}{L_g} & 0 & 0 & 0 & 0 & 0 \\ 0 & 0 & -\omega_s & -\frac{R_g}{L_g} & 0 & \frac{1}{L_g} & 0 & 0 & 0 & 0 \\ \frac{1}{C_f} & 0 & -\frac{1}{C_f} & 0 & 0 & \omega_s & 0 & 0 & 0 & 0 \\ 0 & \frac{1}{C_f} & 0 & -\frac{1}{C_f} & -\omega_s & 0 & 0 & 0 & 0 & 0 \\ 0 & 0 & 0 & 0 & 0 & k_p^{PLL} & -k_p^{PLL} V_{od} & k_i^{PLL} & 0 & 0 \\ 0 & 0 & 0 & 0 & 0 & 1 & -V_{od} & 0 & 0 & 0 \\ -1 & 0 & 0 & 0 & 0 & 0 & -I_{iq} & 0 & 0 & 0 \\ 0 & -1 & 0 & 0 & 0 & 0 & I_{id} & 0 & 0 & 0 \end{bmatrix} \quad (1.68)$$

$$B = \begin{bmatrix} \frac{k_p}{L_f} & 0 & 0 & 0 \\ 0 & \frac{k_p}{L_f} & 0 & 0 \\ 0 & 0 & -\frac{1}{L_g} & 0 \\ 0 & 0 & 0 & -\frac{1}{L_g} \\ 0 & 0 & 0 & 0 \\ 0 & 0 & 0 & 0 \\ 0 & 0 & 0 & 0 \\ 0 & 0 & 0 & 0 \\ 1 & 0 & 0 & 0 \\ 0 & 1 & 0 & 0 \end{bmatrix} \quad (1.69)$$

$$C = \begin{bmatrix} 1 & 0 & 0 & 0 & 0 & 0 & 0 & 0 \\ 0 & 1 & 0 & 0 & 0 & 0 & 0 & 0 \\ 0 & 0 & 1 & 0 & 0 & 0 & 0 & 0 \\ 0 & 0 & 0 & 1 & 0 & 0 & 0 & 0 \end{bmatrix} \quad (1.70)$$

1.5 Impedance model

The Nyquist theory is one of the fundamental tools in studying the stability of linear feedback control systems. In involves plotting the loci of the open loop transfer function of the system in complex plane for frequencies in $(-\infty, \infty)$ range. This plot essentially maps the complex values of the open loop gain in a range of frequencies. To plot the Nyquist graph, a sufficiently large contour is considered that contains the closed right half plane and as s travels on this contour, in clockwise direction, the open loop characteristic loci encircles the $-1 + j0$ point N times, where

$$N_N = Z_N - P_N \tag{1.71}$$

In equation (1.71, Z_N and P_N are zeros and poles of the open loop characteristic function inside the abovementioned contour. The number of unstable closed-loop poles Z_N is equal to the number of unstable open-loop poles P_N plus the number of encirclements of the $-1 + j0$ point. For the system to be stable, Z_N should be zero, resulting in $N_N = -P_N$. This means that for stability, the Nyquist plot should not encircle the $-1 + j0$ point.

This concept of Nyquist stability perfectly predicts the behavior of a single input single output (SISO) systems. In addition, efforts have been made to extend this concept for stability analysis of multi input multi output (MIMO) systems, a proof of which is offered in [11]. In MIMO systems, each output may be affected by several inputs and this coupling interactions are modelled through a matrix. Once again, the open loop characteristic loci of the system is obtained and since this forms a matrix, the loci of eigenvalues of this characteristic are plotted and the focus is on how each eigenvalue loci behaves in the s plane. Essentially, these eigenvalues comprise the modes of the system and analyzing their behavior provides insight into the response of the system's modes.

To apply the GNC to the inverter system, the concept of impedance-based stability analysis is used. Consider that the grid is modelled as an ideal voltage source $V_g(s)$ series with an impedance $Z_g(s)$. As explained in the previous section, the IBR is also modelled as a current source, paralleled with its impedance $Z_{IBR}(s)$. In addition, it is assumed that the grid's voltage source is stable on its own, and when $Z_g(s) = 0$, the IBR's current source is stable as well. With these assumptions, the goal is to derive a condition in which the current in this interconnected system is and remains stable.

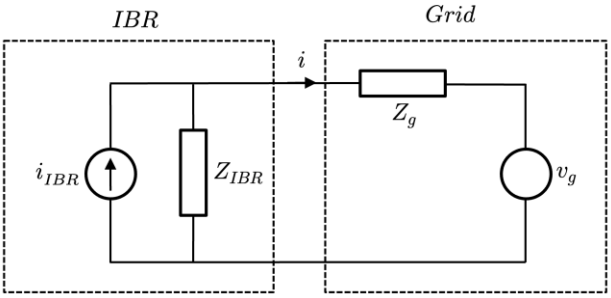

Figure 1-7 Equivalent small signal model of the grid-tied IBR

The current in this model is obtained as follows:

$$I(s) = (I_{IBR}(s) - \frac{v_g(s)}{Z_{IBR}(s)}) \times \frac{1}{1 + Z_g(s)/Z_{IBR}(s)} \tag{1.72}$$

Based on the stability assumption in the previous section, the first term in (1.72 is stable, and if the second term is stable (satisfying the Nyquist stability criterion), the system is stable.

To apply this criterion to the inverter system, the following model for the grid equivalent is developed.

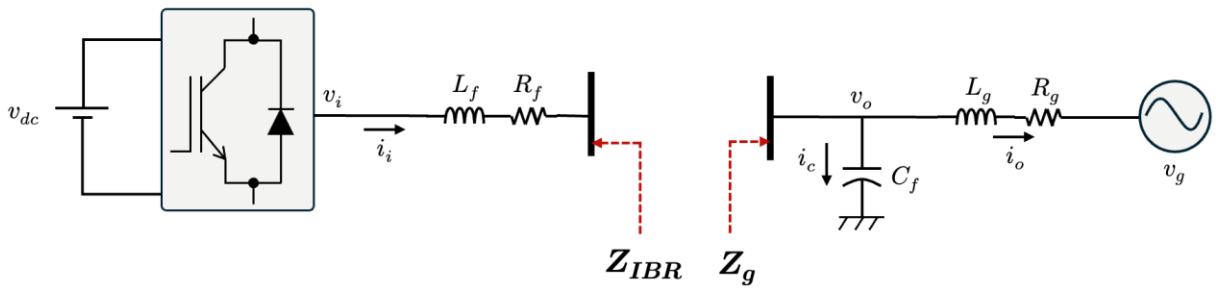

Figure 1-8 Partitioning the grid-tied IBR system for stability analysis

As depicted above, the grid is modelled as a series inductor and resistor. To conduct the stability analysis with the GNC, first the impedance behavior of the IBR, Z_{IBR}, needs to be obtained. Consider the following state space of a standalone IBR:

$$\frac{d}{dt}\begin{bmatrix}\Delta\gamma_d\\ \Delta\gamma_q\\ \Delta i_{id}^s\\ \Delta i_{iq}^s\\ \Delta\theta\\ \Delta\psi\end{bmatrix} = \begin{bmatrix} 0 & 0 & -1 & 0 & -I_q^s & 0\\ 0 & 0 & 0 & -1 & I_d^s & 0\\ \frac{k_i}{L_f} & 0 & -\frac{k_p+R_f}{L_f} & 0 & \frac{-V_{iq}^s+\omega_0 L_f I_d^s-k_p I_q^s}{L_f} & 0\\ 0 & \frac{k_i}{L_f} & 0 & -\frac{k_p+R_f}{L_f} & \frac{V_{id}^s+\omega_0 L_f I_q^s+k_p I_d^s}{L_f} & 0\\ 0 & 0 & 0 & 0 & -k_p^{PLL}V_{od}^s & k_i^{PLL}\\ 0 & 0 & 0 & 0 & -V_{od}^s & 0 \end{bmatrix}\begin{bmatrix}\Delta\gamma_d\\ \Delta\gamma_q\\ \Delta i_{id}^s\\ \Delta i_{iq}^s\\ \Delta\theta\\ \Delta\psi\end{bmatrix} + \begin{bmatrix} 1 & 0 & 0 & 0\\ 0 & 1 & 0 & 0\\ \frac{k_p}{L_f} & 0 & -\frac{1}{L_f} & 0\\ 0 & \frac{k_p}{L_f} & 0 & -\frac{1}{L_f}\\ 0 & 0 & 0 & k_p^{PLL}\\ 0 & 0 & 0 & 1 \end{bmatrix}\begin{bmatrix}\Delta i_{id}^{ref}\\ \Delta i_{iq}^{ref}\\ \Delta v_{od}^s\\ \Delta v_{oq}^s\end{bmatrix} \tag{1.73}$$

$$\begin{bmatrix}\Delta i_{id}^s\\ \Delta i_{iq}^s\end{bmatrix} = \begin{bmatrix}0 & 0 & 1 & 0 & 0 & 0\\ 0 & 0 & 0 & 1 & 0 & 0\end{bmatrix}\begin{bmatrix}\Delta\gamma_d\\ \Delta\gamma_q\\ \Delta i_{id}^s\\ \Delta i_{iq}^s\\ \Delta\theta\\ \Delta\psi\end{bmatrix} \tag{1.74}$$

To develop the admittance behavior of this system, the following transfer function, $G = \frac{y}{U} = C \times (sI - A)^{-1}B$, based on the abovementioned state space.

$$\begin{bmatrix}\Delta i_{id}^s\\ \Delta i_{iq}^s\end{bmatrix} = \begin{bmatrix}G_{11} & G_{12} & G_{13} & G_{14}\\ G_{21} & G_{22} & G_{23} & G_{24}\end{bmatrix}\begin{bmatrix}\Delta i_{id}^{ref}\\ \Delta i_q^{ref}\\ \Delta v_{od}^s\\ \Delta v_{oq}^s\end{bmatrix} \tag{1.75}$$

Since the system is linear hence superposition rule holds, by assuming $\Delta i_{id}^{ref} = \Delta i_{iq}^{ref} = 0$, the admittance of the inverter as a function of frequency as follows:

$$Y_{IBR} = Z_{IBR}^{-1} = \begin{bmatrix} Y_{dd} & Y_{dq} \\ Y_{qd} & Y_{qq} \end{bmatrix} = \begin{bmatrix} G_{13} & G_{14} \\ G_{23} & G_{24} \end{bmatrix} \tag{1.76}$$

$$Y_{dd} = -\frac{s}{k_i + (R_f + k_p)s + L_f s^2} \tag{1.77}$$

$$Y_{dq} = -\frac{I_{iq}k_i k_i^{PLL} + \left(V_{iq}k_i^{PLL} + I_{iq}k_i k_p^{PLL} + I_{iq}k_i^{PLL}k_p - I_{id}L_f k_i^{PLL}\right)s + \left(V_{iq}k_p^{PLL} + I_{iq}k_p k_p^{PLL} - I_{id}L_f k_p^{PLL}\omega_s\right)s^2}{(s^2 + V_{od}k_p^{PLL}s + V_{od}k_i^{PLL})(k_i + (R_f + k_p)s + L_f s^2)} \tag{1.78}$$

$$Y_{qd} = 0 \tag{1.79}$$

$$Y_{qq} = \frac{I_{id}k_i k_i^{PLL} + (V_{id}k_i^{PLL} - V_{od}k_i^{PLL} + I_{id}k_i k_p^{PLL} + I_{id}k_p k_i^{PLL} - I_{iq}L_f k_i^{PLL}\omega_s)s + (V_{id}k_p^{PLL} - V_{od}k_p^{PLL} + I_{id}k_p k_p^{PLL} + I_{iq}L_f k_p^{PLL}\omega_s)s^2 - s^3}{(s^2 + V_{od}k_p^{PLL}s + V_{od}k_i^{PLL})(k_i + (R_f + k_p)s + L_f s^2)} \tag{1.80}$$

Now that the admittance is derived, the impedance ratio can be formed, and the eigenvalues are obtained as follows:

$$L = Z_g(s) \times Y_{IBR}(s) = \begin{bmatrix} L_{11}(s) & L_{12}(s) \\ L_{21}(s) & L_{22}(s) \end{bmatrix} \tag{1.81}$$

$$\begin{pmatrix} e_1(s) \\ e_2(s) \end{pmatrix} = \frac{1}{2} \times \begin{pmatrix} L_{11}(s) + L_{22}(s) - \sqrt{L_{11}^2(s) - 2L_{11}(s)L_{22}(s) + L_{22}^2(s) + 4L_{12}(s)L_{21}(s)} \\ L_{11}(s) + L_{22}(s) + \sqrt{L_{11}^2(s) - 2L_{11}(s)L_{22}(s) + L_{22}^2(s) + 4L_{12}(s)L_{21}(s)} \end{pmatrix} \tag{1.82}$$

The loci of these eigenvalues are utilized to study the stability of the grid-tied IBR system.

1.6 LVRT grid code

Figure 1-9 a) and Figure 1-9 b) demonstrate typical requirements for the operation of IBRs in facing faults that cause voltage sags.

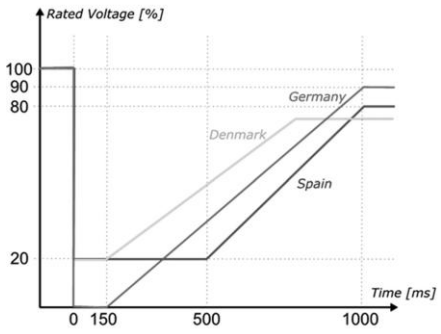

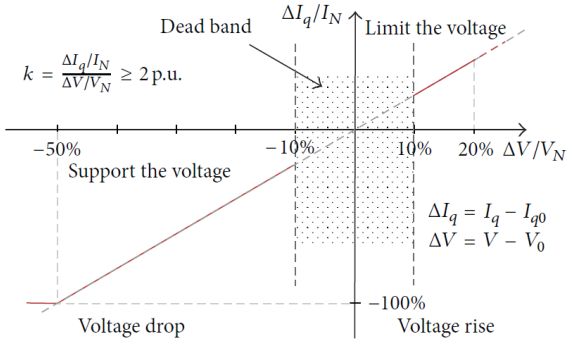

a) b)

Figure 1-9 a) LVRT requirement in Germany, Denmark, and Spain b) Reactive power requirement grid code upon low voltage events [12]

The current output of the inverter must also be limited to a certain maximum value, as stated in (1.83.

$$\sqrt{I_{id}^2 + I_{iq}^2} < I_{max} \tag{1.83}$$

Where $I_{max} = kI_n$, where I_n is the nominal current of the inverter and k is typically equal to 1.2. similar constraints are considered for the voltage as follows:

$$\sqrt{v_{id}^2 + v_{iq}^2} < V_{max} \tag{1.84}$$

With these limitations in mind, in this project the LVRT logic is implemented as follows.

ALGORITHM 1: LVRT LOGIC

Input v_{id}
$\boldsymbol{I_{iq}^{check} = 2(1 - v_{id})I_N}$
If $v_{id} > 0.9$
    $I_{iq}^{modified} = I_{iq}^{ref}$; $I_{id}^{modified} = I_{id}^{ref}$
If $v_{id} \leq 0.9$
    If $I_q^{check} \geq I_{max}$
        $I_{iq}^{modified} = I_{max}$; $I_d^{modified} = 0$
    If $I_q^{check} < I_{max}$
        $I_q^{modified} = I_q^{check}$
        If $I_d^{no\ limit} \geq \sqrt{I_{max}^2 - \left(I_q^{check}\right)^2}$
            $I_d^{modified} = \sqrt{I_{max}^2 - \left(I_q^{check}\right)^2}$
        If $I_d^{no\ limit} < \sqrt{I_{max}^2 - \left(I_q^{check}\right)^2}$
            $I_d^{modified} = I_d^{no\ limit}$

1.7 Numerical analysis

The analysis is conducted in two sections. First, case studies are designed to examine and compare the effectiveness of the two stability analysis tools to understand how the strength of the grid can affect the synchronization stability of the grid-tied IBR system. In the second part, time domain simulations are conducted to study the effect of delay in the LVRT grid code on the TOV given various grid strengths.

1.7.1 Grid Synchronization Stability analysis

In this section, a test system with the parameters shown in Table 1 is studied.

Table 1 Parameters of the VSC

Parameter	Value
k_p	0.023
k_i	25.59
k_p^{PLL}	4.46, 8.92, 17.84
k_i^{PLL}	991, 3964, 15860
ω_s	$2\pi \times 60\, rad/s$
R_f	120 $m\Omega$
L_f	970 μH
C_f	10 μF
I_{id}^s	-11 Amp
I_{iq}^s	0 Amp
v_{id}^s	100 v
v_{iq}^s	0 v
v_{od}^s	99.9 v
v_{oq}^s	0 v

To start with, the impedance/admittance behavior of the IBR is studied. This admittance was derived in (1.76. To understand the effect of PLL bandwidth on the impedance behavior, three different sets of PLL parameters in the increasing order. The results are as follows:

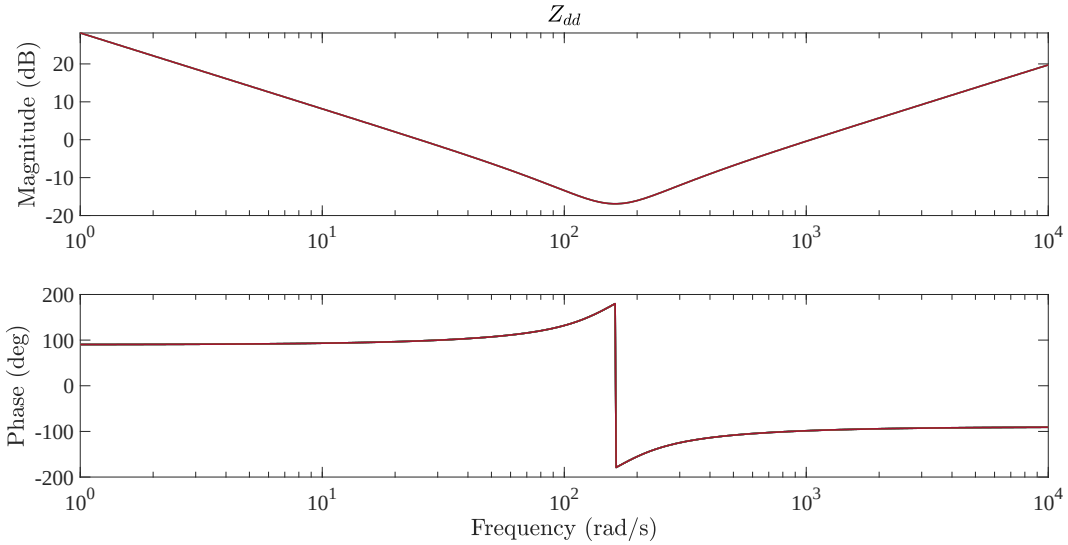

Figure 1-10 dd channel impedance of the IBR

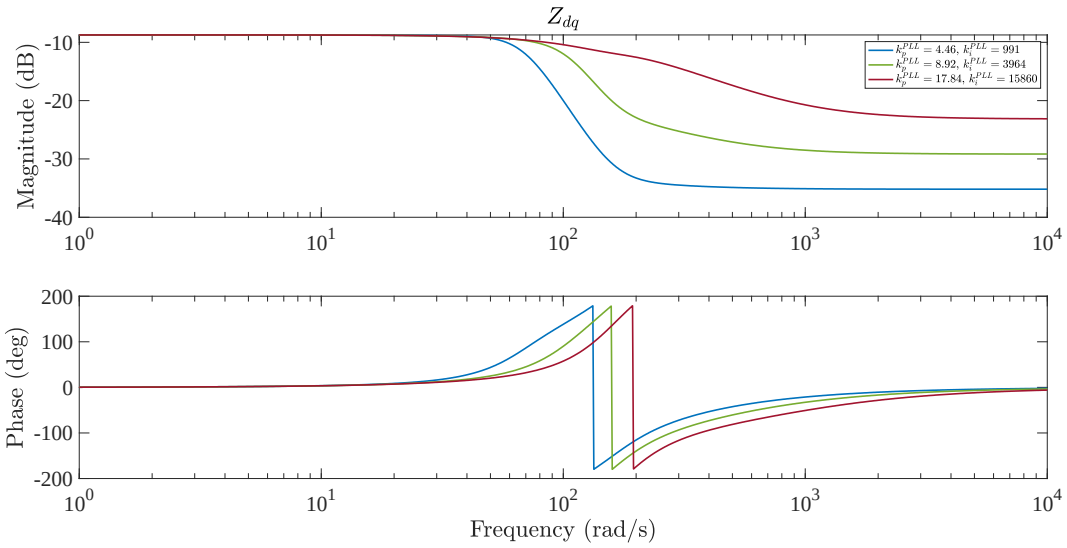

Figure 1-11 dq channel impedance of the IBR

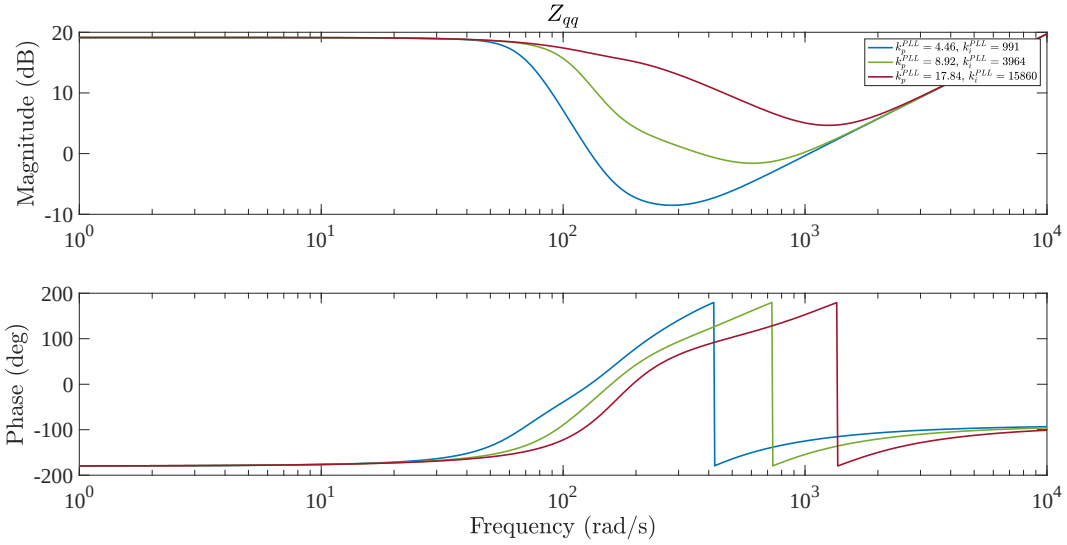

Figure 1-12 qq channel impedance of the IBR

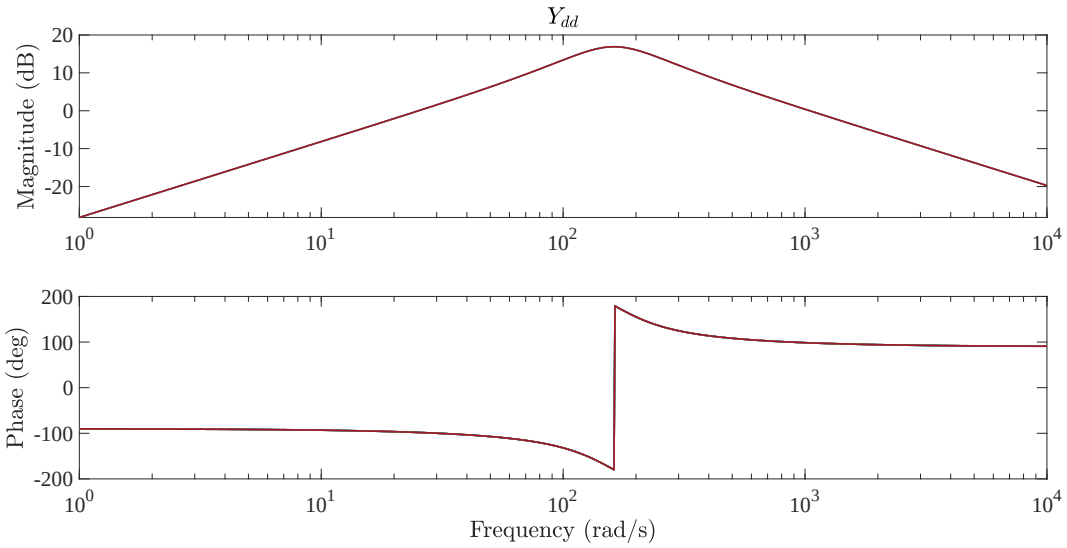

Figure 1-13 dd channel admittance of the IBR

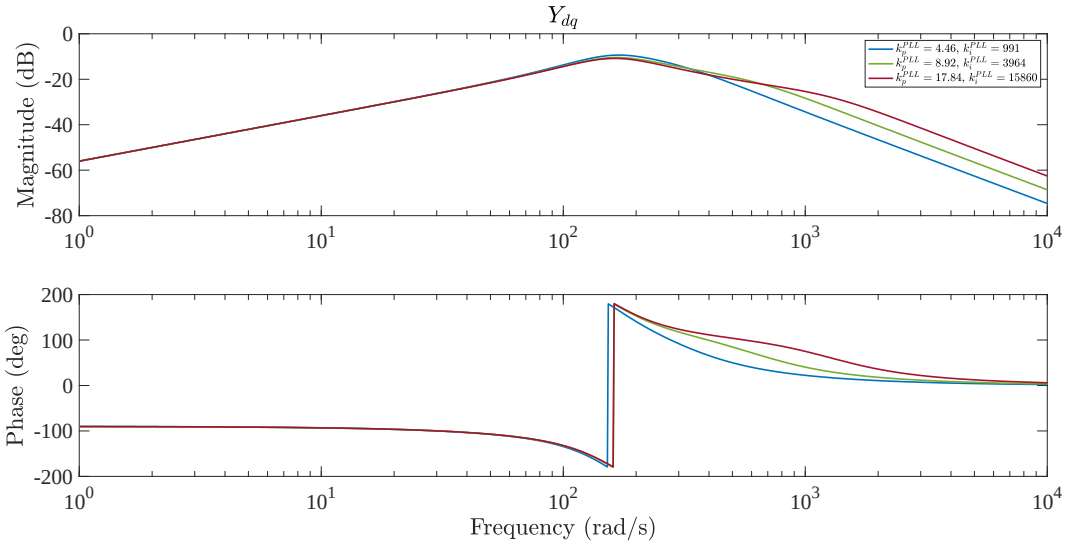

Figure 1-14 dq channel admittance of the IBR

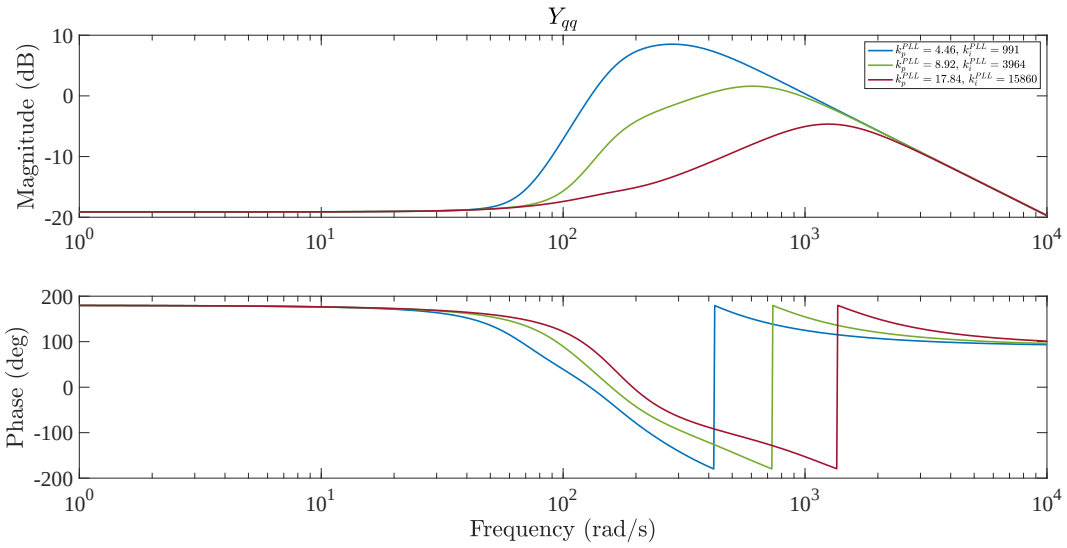

Figure 1-15 qq channel admittance of the IBR

The main takeaway from these impedance behaviors is that the matrix is close to diagonal, as the qd channel is zero, and the dq channel is sufficiently small. In addition, the qq channel acts as a negative resistance where the bandwidth of the PLL determines the range of frequency for this behavior, as depicted in Figure 1-12.

Next, this IBR is synchronized with a grid and the effect of various grid strengths on the grid synchronization stability of the IBR system is studied.

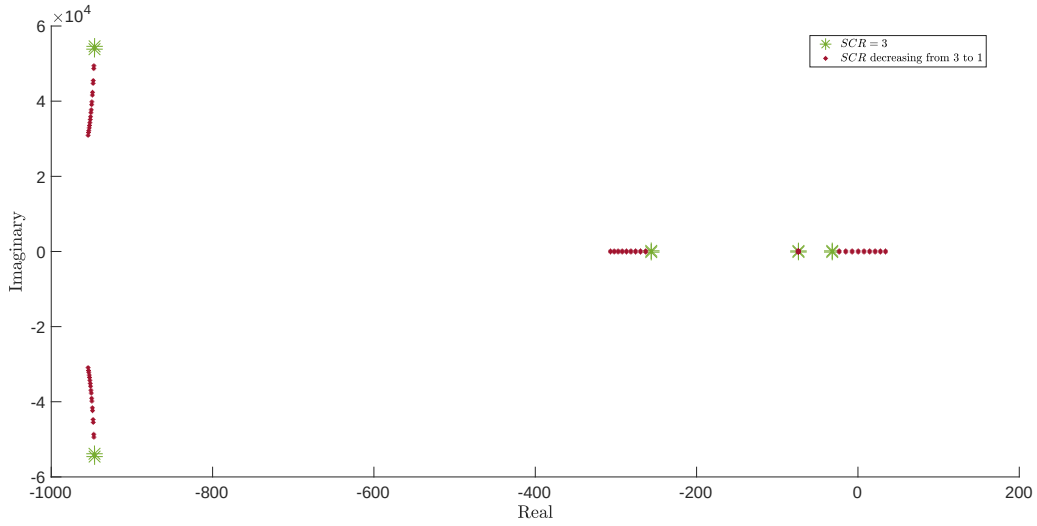

Figure 1-16 Eigenvalues of the grid-tied IBR system as a function of grid strength.

As shown in Figure 1-16, when the grid is strong, the interconnection is stable. The system as modelled in (1.68 has 10 modes, and when $\mathtt{SCR} = 3$ (the green dots in Figure 1-16), the system is

small signal stable. This is also verified in the GNC plot of the system in Figure 1-17, as the eigenvalues do not cross the critical point.

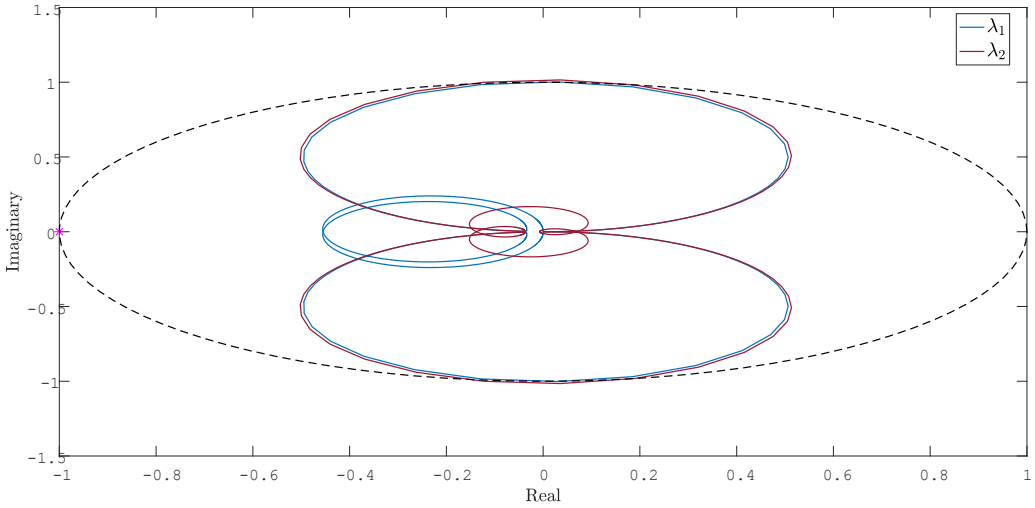

Figure 1-17 GNC plot of the grid-tied IBR system at $\mathrm{SCR} = 3$

Next, the grid strength has been reduced. As depicted in Figure 1-16, as the grid becomes weaker (higher impedance) at some point the two modes on the right cross the $j\omega$ axis which indicates the loss of synchronism and instability of the system. This result is also verified using the following three GNC plots in Figure 1-18, Figure 1-19, and Figure 1-20. As the strength decreases, λ_1 moves towards the critical point and as shown in Figure 1-20, at $\mathrm{SCR} = 1$ the loci encircles the critical point twice.

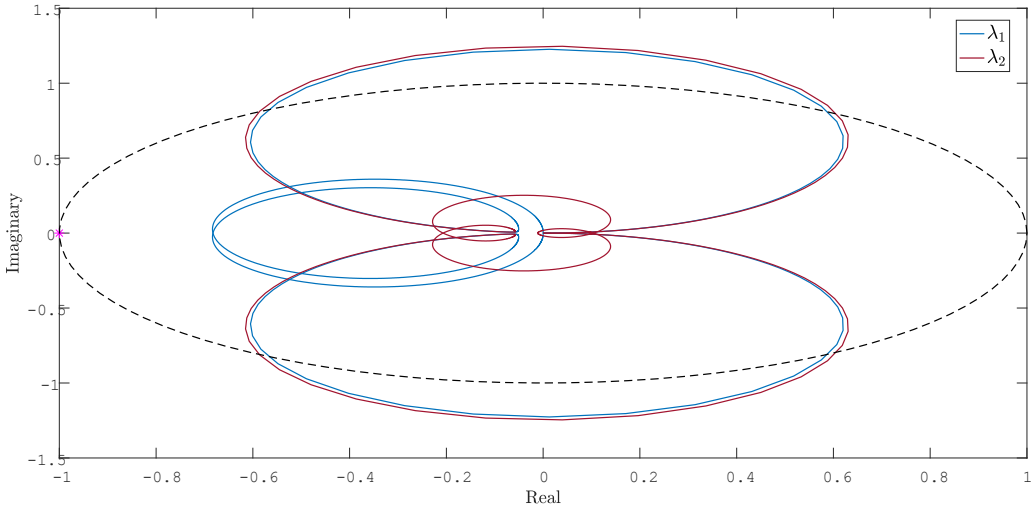

Figure 1-18 GNC plot of the grid-tied IBR system at $\mathrm{SCR} = 2$

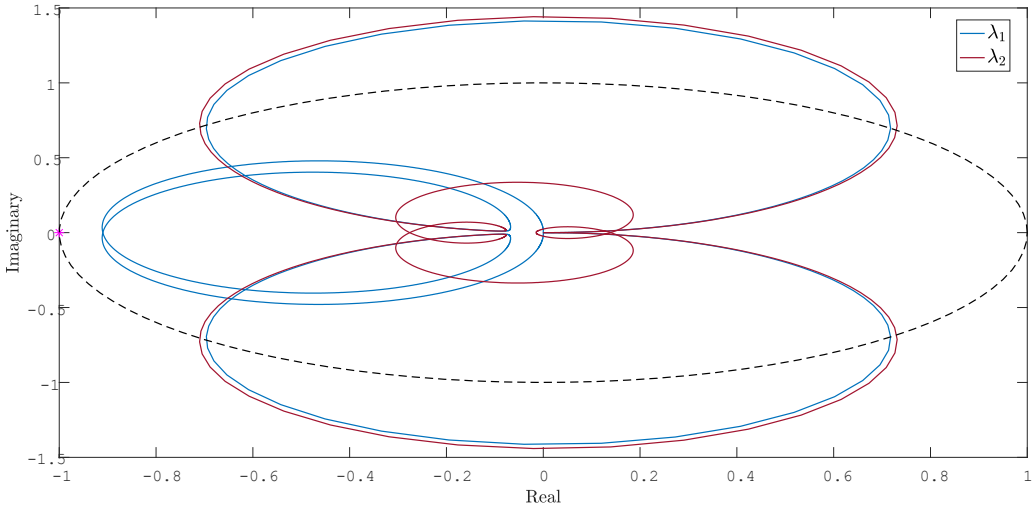

Figure 1-19 GNC plot of the grid-tied IBR system at $\mathrm{SCR} = 1.5$

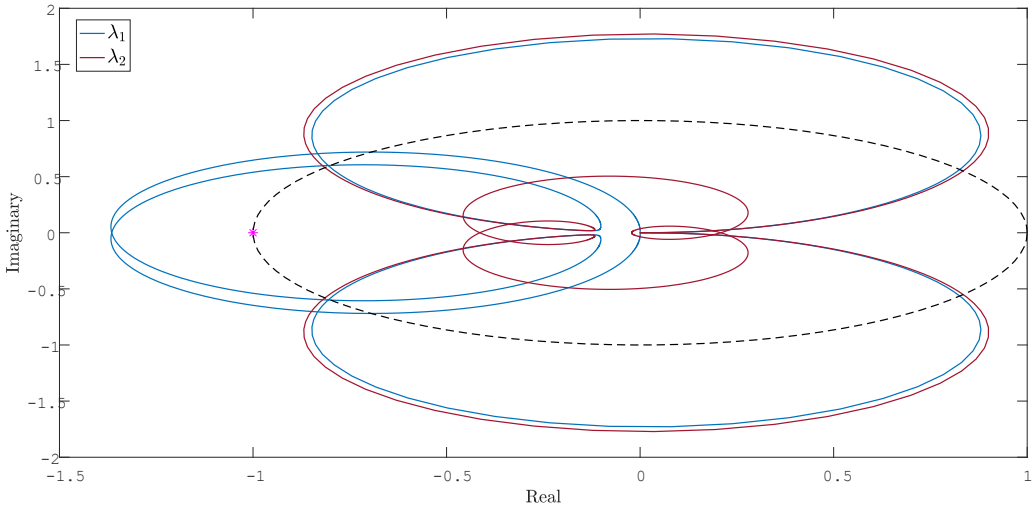

Figure 1-20 GNC plot of the grid-tied IBR system at $\mathrm{SCR} = 1$

1.7.2 Time domain simulations

In this section impact of delay in the LVRT logic and grid strength are studied. The delays are related to the time required by the LVRT to detect the exact fault clearance time to switch between during fault and post fault conditions. To start with, the grid-tied IBR system as depicted in Figure 1-21 is simulated in MATLAB/Simulink®, the difference being that the IBR is connected to the grid via two identical transmission lines. In this system, $S_{IBR} = 100\ kVA$, and the output voltage of the inverter is 500 v. The IBR is connected to the grid via two identical transmission lines where the voltage is boosted and decreased at the terminals of the transmission lines via a 500⁄69 kV and a 69⁄500 V transformers, respectively. In addition, a PLL is utilized to track the grid's angle and

frequency, based on which the IBR controller operates. A three-phase symmetrical fault occurs on one of the transmission lines at $t = 0.2\ s$. This fault is cleared after $0.1\ s$. In the first scenario, it is assumed that the grid is strong ($\mathrm{SCR} = 20$), and the fault is cleared by itself, hence, the grid's strength remains unchanged. Once a voltage sag is detected, the LVRT is used based on Algorithm 2.

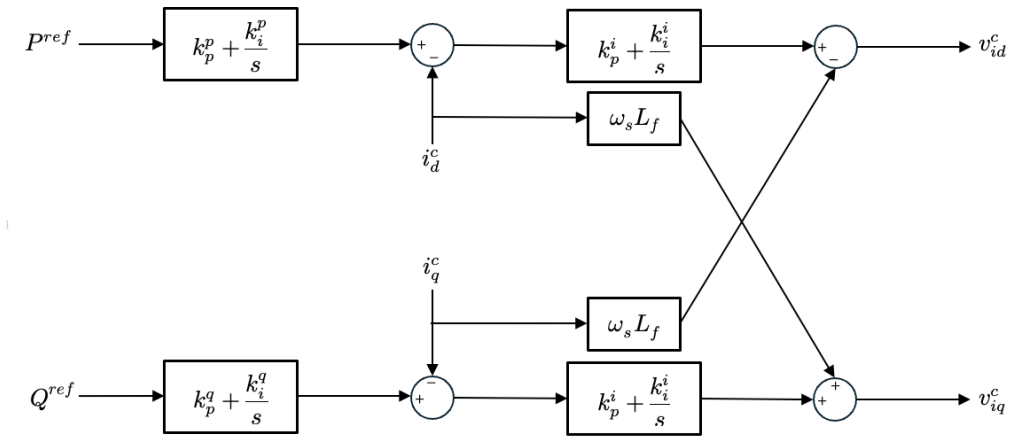

Figure 1-21 cascaded inner/outer control loops

First, assume an operating condition where there is zero controller action delay. The grid is strong (SCR = 20), and a three-phase symmetrical fault occurs on one of the lines at 0.2 s, and lasts for 0.01 s (Case 1). Figure 1-22 shows the voltage profile at POI.

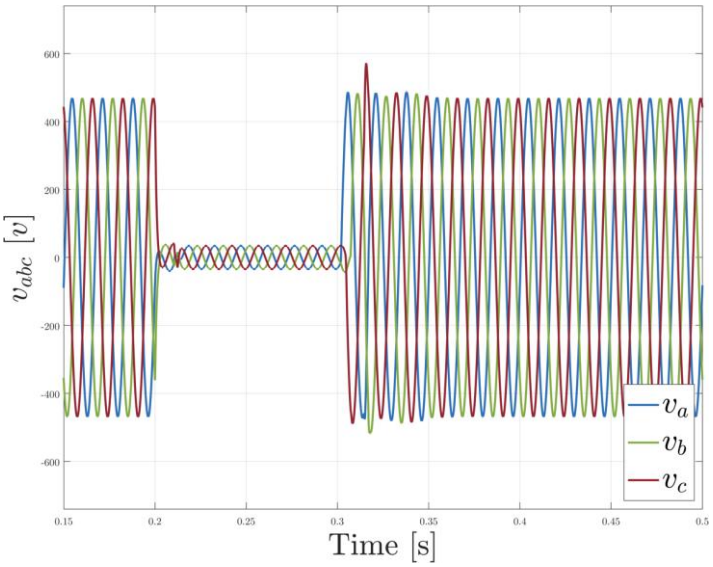

Figure 1-22 Case one with zero delay, max is $572.5\ v$, steady state $469.5\ v$

Next, a $5\ ms$ delay is introduced to the LVRT grid code action. This indicates that for $5\ ms$ after the fault clearance, the IBR keeps on injecting reactive power to support the grid as depicted in Figure 1-23. Same results are also presented with $10\ ms$, $20\ ms$, and $30\ ms$ delay in Figure 1-24, Figure 1-25, and Figure 1-26, respectively. It is shown that in a strong grid interconnection, the TOV duration is proportional to the delay, but this relationship is not necessarily linear.

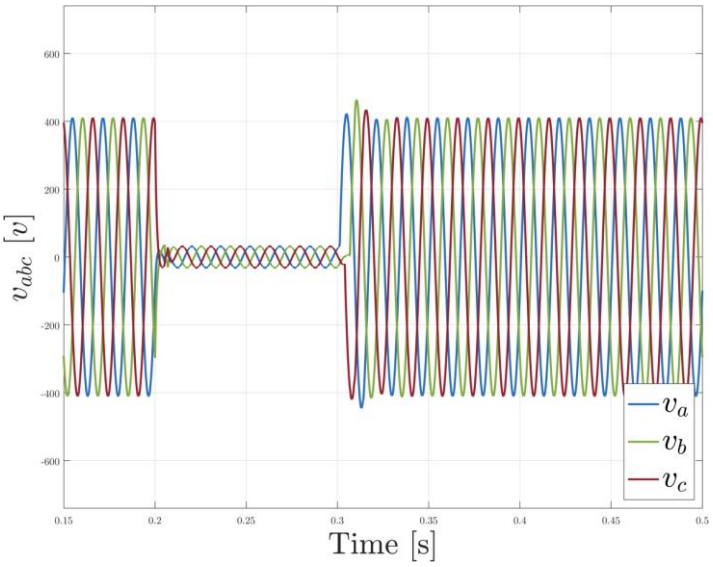

Figure 1-23 Case one with $5\ ms$ delay, max is $464.5\ v$, steady state $410\ v$

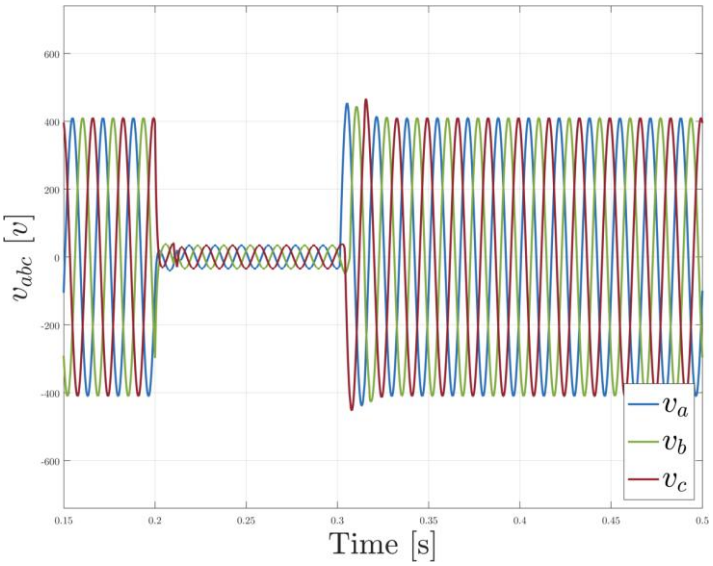

Figure 1-24 Case one with $10\ ms$ delay, max is $467.5\ v$, steady state $412\ v$

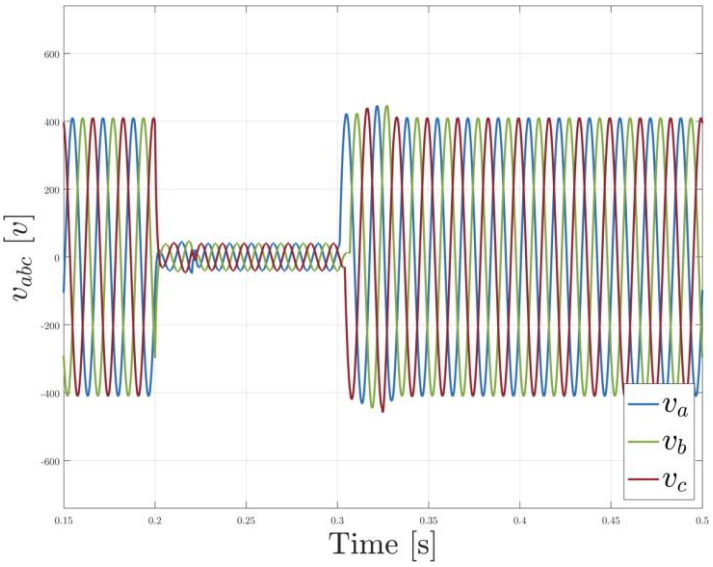

Figure 1-25 Case one with $20\,ms$ delay, max is $448.5\,v$, steady state $412\,v$

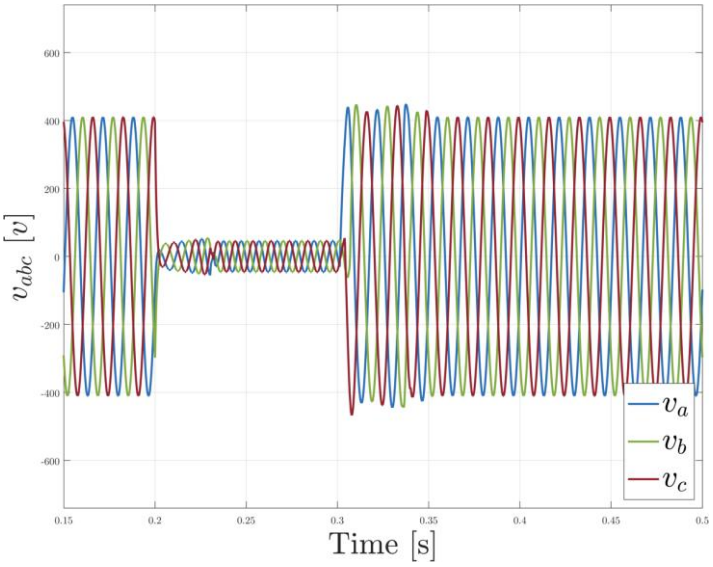

Figure 1-26 Case one with $30\,ms$ delay, max is $448.5\,v$, steady state $412\,v$

Next, it is assumed that the grid is weak, and after fault clearance, the strength remains unchanged. In the following analysis, SCR = 1 at pre fault, during fault, and post fault (Case 2). The TOV results for different delays are depicted in Figure 1-27 and Figure 1-28. The TOV magnitude and severity are worse than the strong grid and possible instable condition may occur. The strong grid can accommodate a faster PLL and tolerate longer delays, unlike the weak system. For instance, any delay longer than $10\,ms$ causes the IBR loses its synchronism.

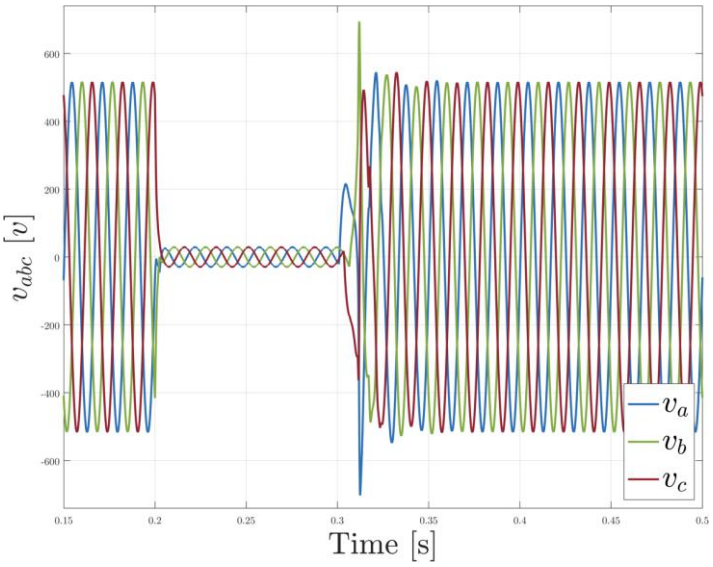

Figure 1-27 Case two with $0\ ms$ delay, max is $695.5\ v$, steady state $517\ v$

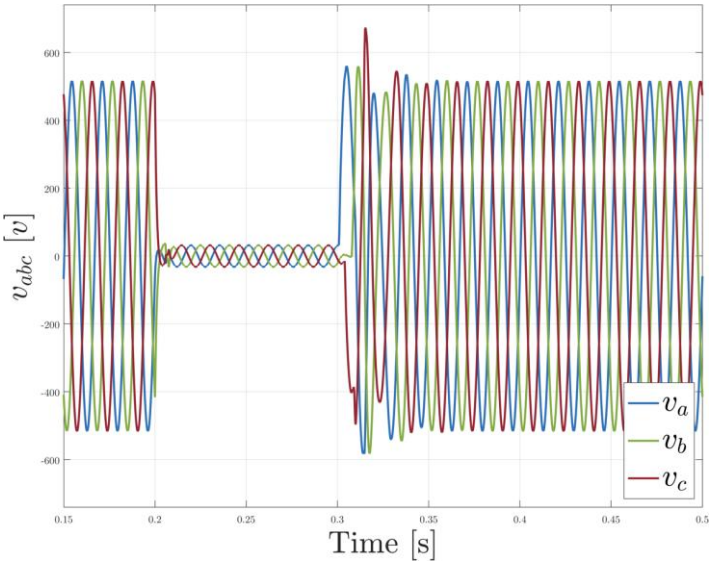

Figure 1-28 Case two with $5\ ms$ delay, max is $673.5\ v$, steady state $517\ v$

Another case that is investigated is when the strength changes after the fault clearance (Case 3) in which the faulted lone is taken out of service to clear the fault. As depicted in Figure 1-29 to Figure 1-32, compared to the two other cases, the change in the grid's strength causes a more severe TOV.

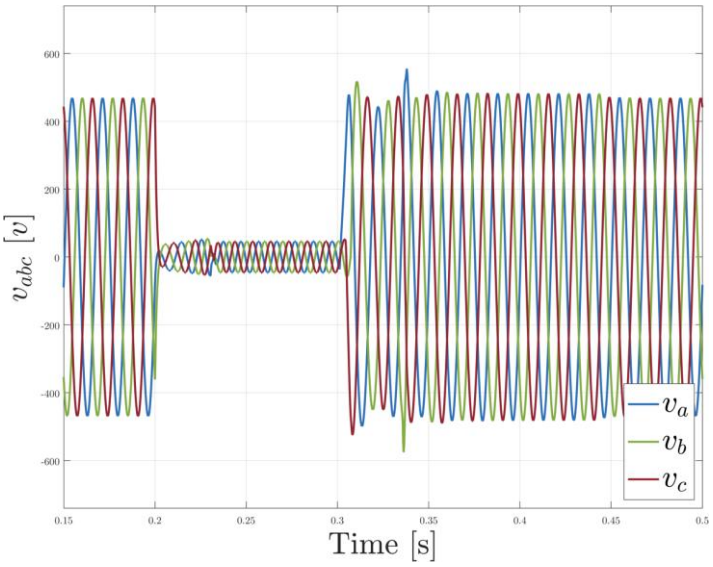

Figure 1-29 Case three with $0\ ms$ delay, max is $556.5\ v$, steady state $468\ v$

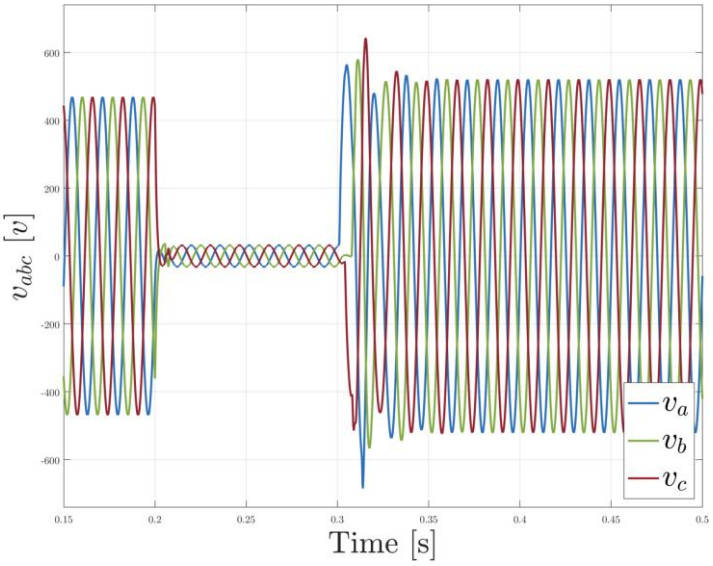

Figure 1-32 Case three with $5\ ms$ delay, max is $643.5\ v$, steady state $521\ v$

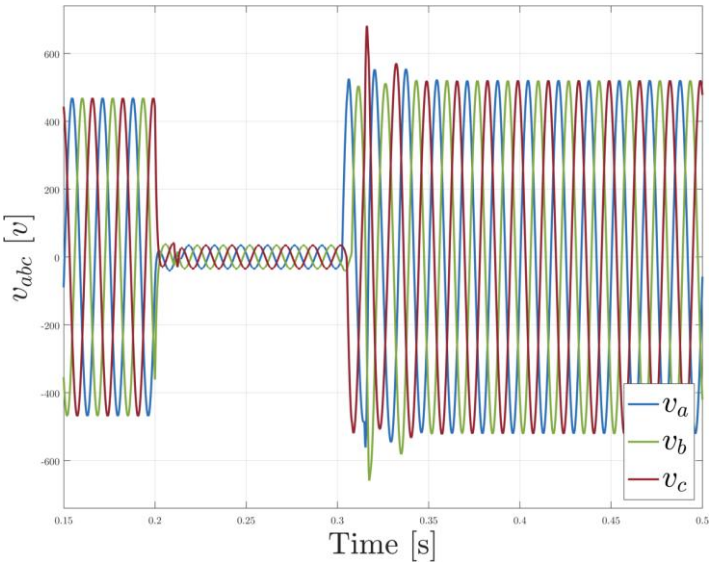

Figure 1-30 Case three with $10\,ms$ delay, max is $682.5\,v$, steady state $521\,v$

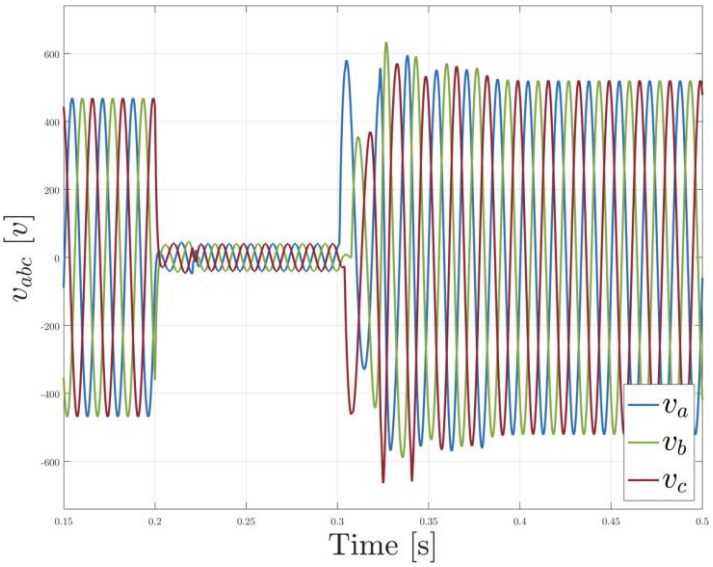

Figure 1-31 Case three with $20\,ms$ delay, max is $665.5\,v$, steady state $521\,v$

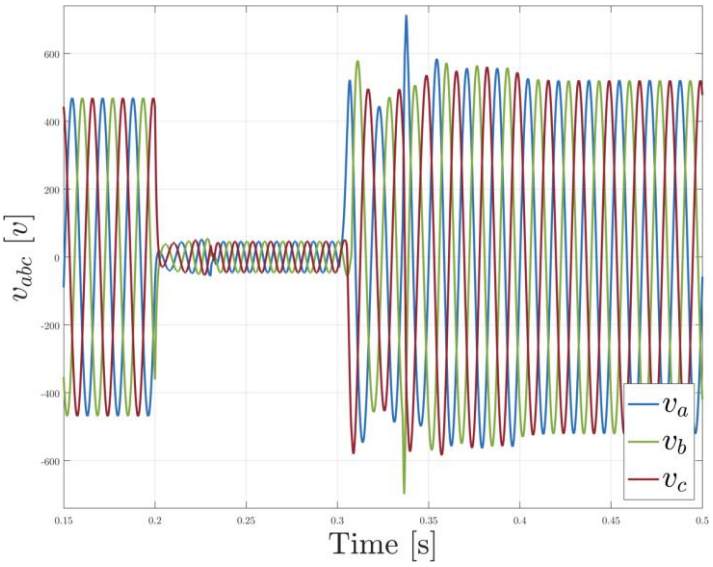

Figure 1-32 Case three with $30\,ms$ delay, max is $413.5\,v$, steady state $521\,v$

In addition, the effect of PLL dynamics is investigated. In Case 1, in the presence of $20\,ms$ delay, the PLL bandwidth is increased from $484.13\,Hz$ to $4110.3\,Hz$, which is the maximum PLL speed for which the system to remain stable during the post fault. The TOV profile is depicted in Figure 1-33. Next, for the same setup, in Case three, the PLL bandwidth is increased to $1686.2\,Hz$. As stated before, in a weak grid, the PLL bandwidth is limited compared to a strong grid. In addition, weaker grids exhibit larger TOVs and a higher risk of synchronization instability, as depicted in Figure 1-34 and Figure 1-35.

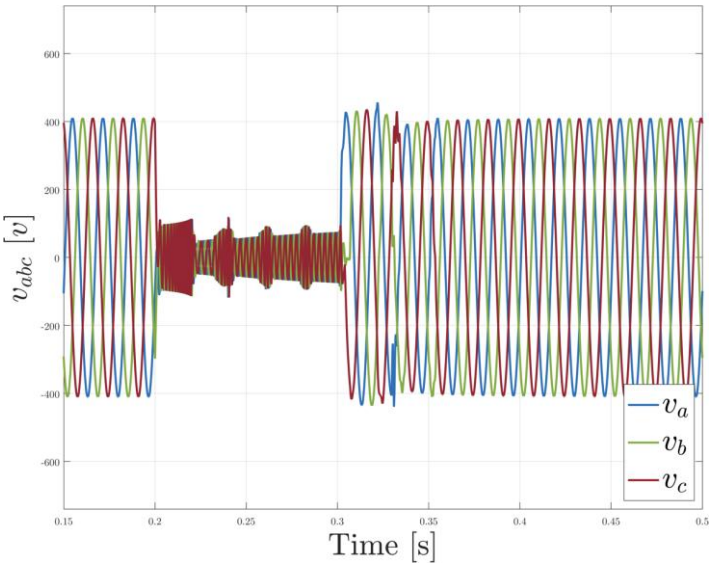

Figure 1-33 Case one with $20\,ms$ delay, max is $453.5\,v$, steady state $412\,v$, faster PLL

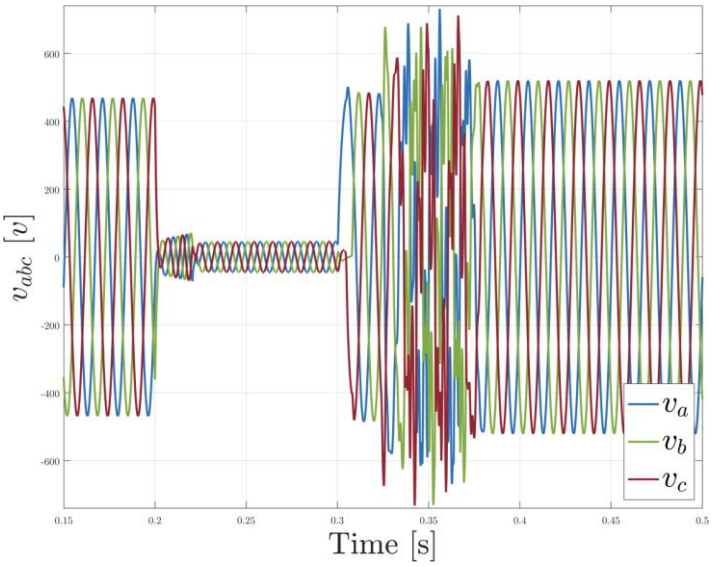

Figure 1-34 Case three with $20\ ms$ delay, max is $732.5\ v$, steady state $521\ v$, faster PLL

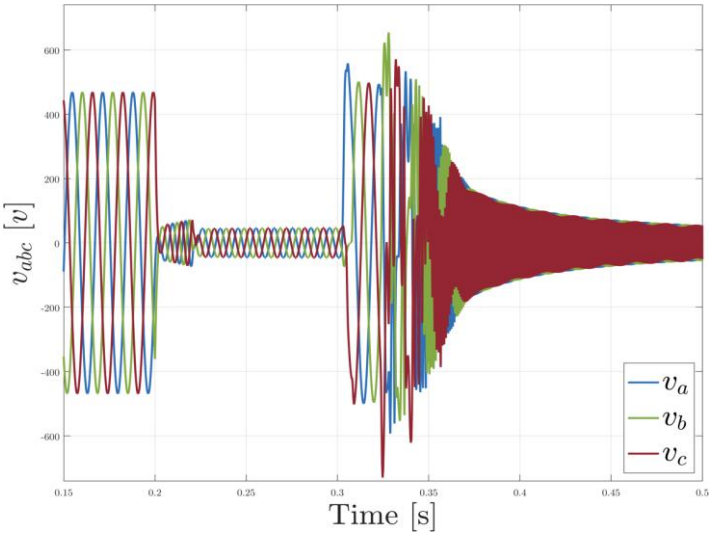

Figure 1-35 Case three, instability with faster PLL bandwidth

1.8 Conclusions

In this report, the TOV phenomenon caused by IBR dominated power systems was studied in detail. Given that grid strength is directly correlated with numerous issues caused by GFL IBRs, a thorough study and comparison of various strength indices were conducted. Since the conventional SCR fails to measure grid strength in many different configurations, it is crucial to choose an approach that captures the desired dynamics of the grid under study. Subsequently, a model-based approach was developed to calculate the impedance behavior of the grid-tied IBR system. Stability analysis using GNC, and conventional eigenvalue analysis was performed, and the results of each method were cross-checked. Finally, a time-domain simulation was conducted to perform a

parametric study on the effects of controller action delay in causing TOVs at the POI. The results validate that weak systems exhibit more severe TOVs and are prone to loss of synchronism.

References

[1] "IEEE Recommended Practice for Surge Voltages in Low-Voltage AC Power Circuits," *IEEE Std C6241-1991*, pp. 1–112, Oct. 1991, doi: 10.1109/IEEESTD.1991.101029.

[2] "Risk Assessment of Post-Fault Temporary Overvoltage Using Generalized Short-Circuit Ratio | IEEE Journals & Magazine | IEEE Xplore." Accessed: Feb. 19, 2024. [Online]. Available: https://ieeexplore.ieee.org/document/10035300

[3] "RAPA - Short-Circuit Modeling and System Strength..." Accessed: May 17, 2024. [Online]. Available: https://www.nerc.com/pa/RAPA/Lists/RAPA/DispForm.aspx?id=291&Source=https://www.nerc.com/pa/RAPA/Pages/Calendar.aspx

[4] M. O. Qays, I. Ahmad, D. Habibi, A. Aziz, and T. Mahmoud, "System strength shortfall challenges for renewable energy-based power systems: A review," *Renew. Sustain. Energy Rev.*, vol. 183, p. 113447, Sep. 2023, doi: 10.1016/j.rser.2023.113447.

[5] "Systems with multiple DC Infeed." Accessed: Jun. 04, 2024. [Online]. Available: https://www.e-cigre.org/publications/detail/364-systems-with-multiple-dc-infeed.html

[6] D. Wu, G. Li, M. Javadi, A. M. Malyscheff, M. Hong, and J. N. Jiang, "Assessing Impact of Renewable Energy Integration on System Strength Using Site-Dependent Short Circuit Ratio," *IEEE Trans. Sustain. Energy*, vol. 9, no. 3, pp. 1072–1080, Jul. 2018, doi: 10.1109/TSTE.2017.2764871.

[7] "Connection of wind farms to weak AC networks." Accessed: Apr. 15, 2024. [Online]. Available: https://www.e-cigre.org/publications/detail/671-connection-of-wind-farms-to-weak-ac-networks.html

[8] C. Henderson, A. Egea-Alvarez, T. Kneuppel, G. Yang, and L. Xu, "Grid Strength Impedance Metric: An Alternative to SCR for Evaluating System Strength in Converter Dominated Systems," *IEEE Trans. Power Deliv.*, pp. 1–10, 2023, doi: 10.1109/TPWRD.2022.3233455.

[9] P. O. Dorile, D. R. Jagessar, L. Guardado, R. A. McCann, and M. Ahanch, "Grid Strength Assessment and Maximum Loadability of a Wind-Dominated Power System Through QV Modal Analysis," in *2021 IEEE PES/IAS PowerAfrica*, Aug. 2021, pp. 1–5. doi: 10.1109/PowerAfrica52236.2021.9543346.

[10] G. Wang, H. Xin, D. Wu, Z. Li, L. Huang, and P. Ju, "Generalized Short Circuit Ratio for Grid Strength Assessment in Inhomogeneous Multi-infeed LCC-HVDC Systems," Dec. 18, 2020, *arXiv*: arXiv:2011.07564. doi: 10.48550/arXiv.2011.07564.

[11] A. G. J. MAcFARLANE and I. POSTLETHWAITE, "The generalized Nyquist stability criterion and multivariable root loci," *Int. J. Control*, vol. 25, no. 1, pp. 81–127, Jan. 1977, doi: 10.1080/00207177708922217.

[12] M. Diaz, R. Cardenas, P. Wheeler, J. Clare, and F. Rojas, "Resonant Control System for Low-Voltage Ride-Through in Wind Energy Conversion Systems," *IET Power Electron.*, vol. 9, Feb. 2016, doi: 10.1049/iet-pel.2015.0488.